

Periodicity detection in the broad line and continuum light curves of active galactic nuclei

A. Kovačević¹, L. Č. Popović^{1,2}, D. Ilić¹

¹ Department of astronomy, Faculty of Mathematics, University of Belgrade, Serbia

² Astronomical Observatory Belgrade, Serbia

symmetry in time

- extracting energy from environment: oscillators and generators, heartbeats
- bearing information: i.e circular orbit or elliptical orbit, oscillations in CPUs

fractals in time

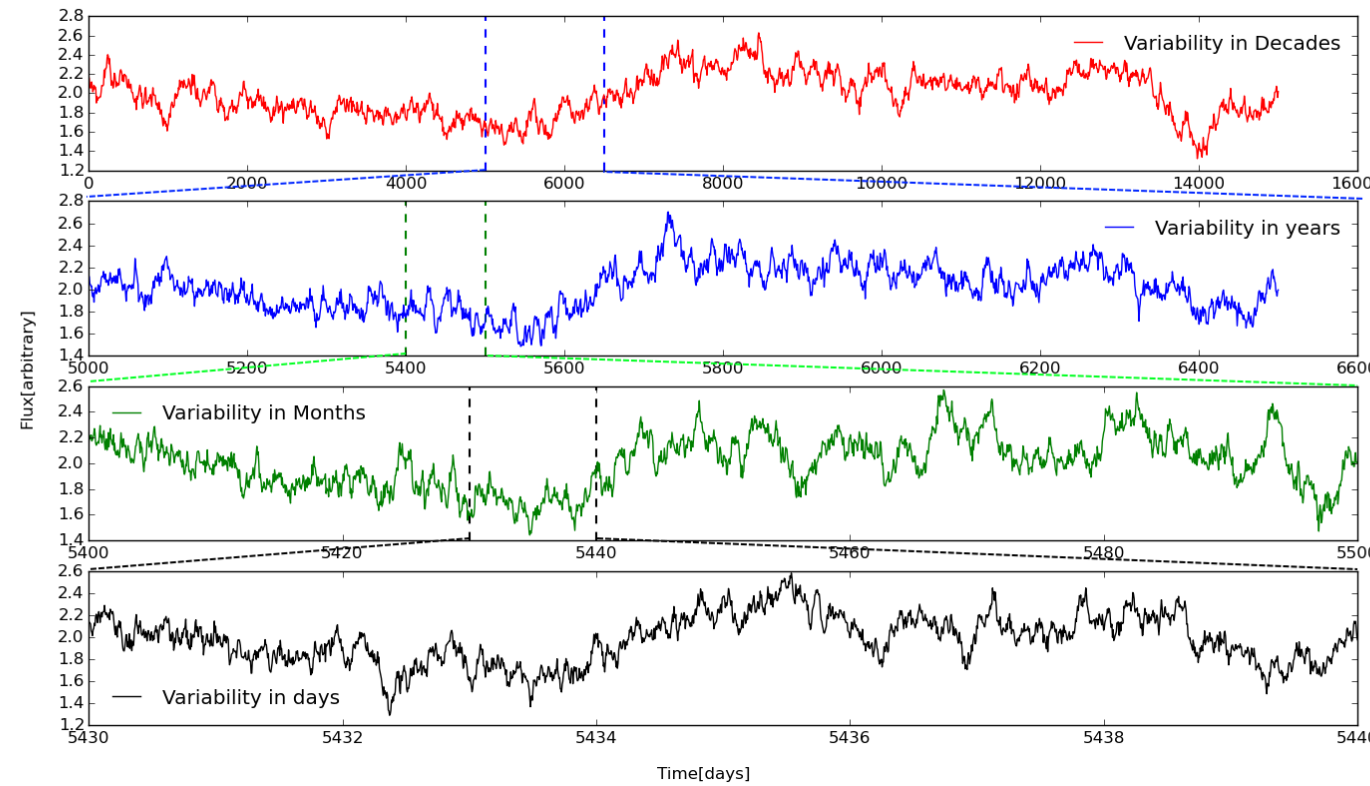


Figure 1.5.: Representation of AGN light curves at different time scales.

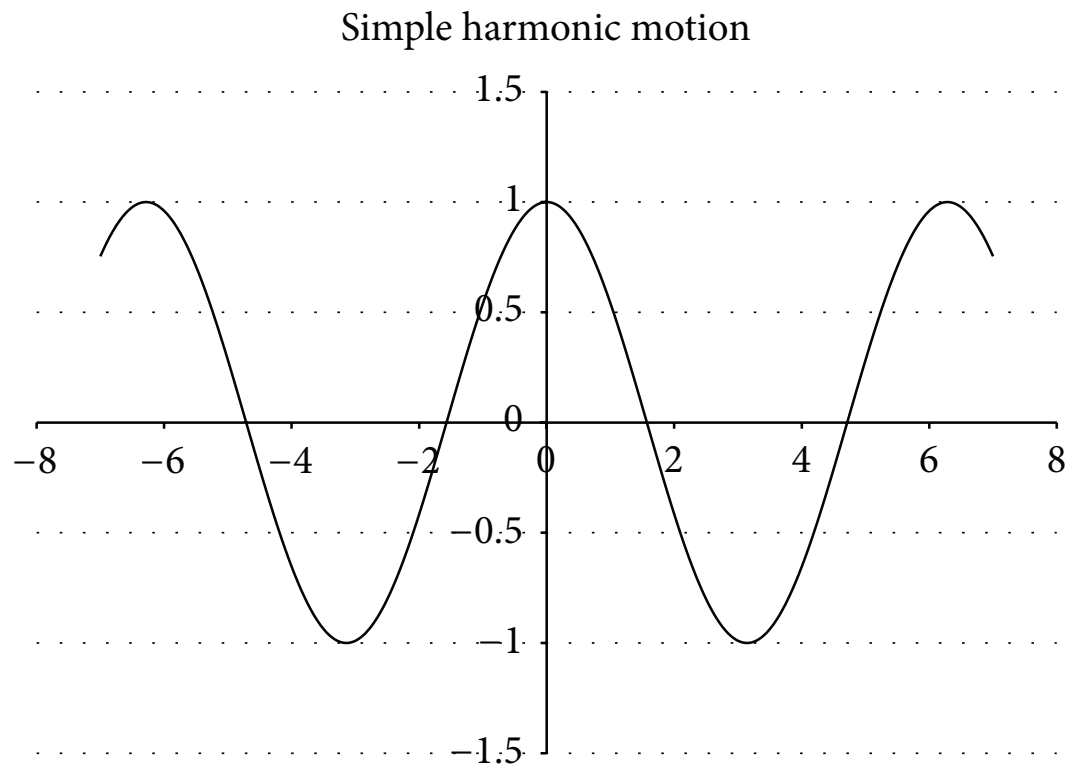


FIGURE 1: Position versus time for the simple harmonic oscillator.

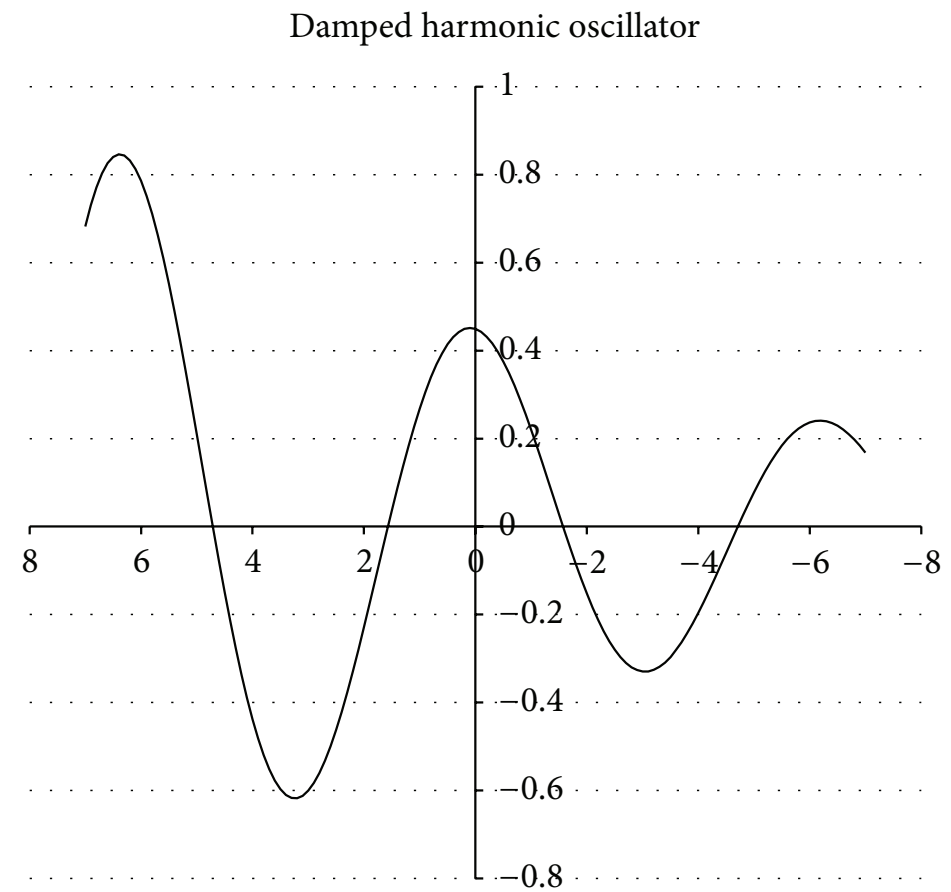


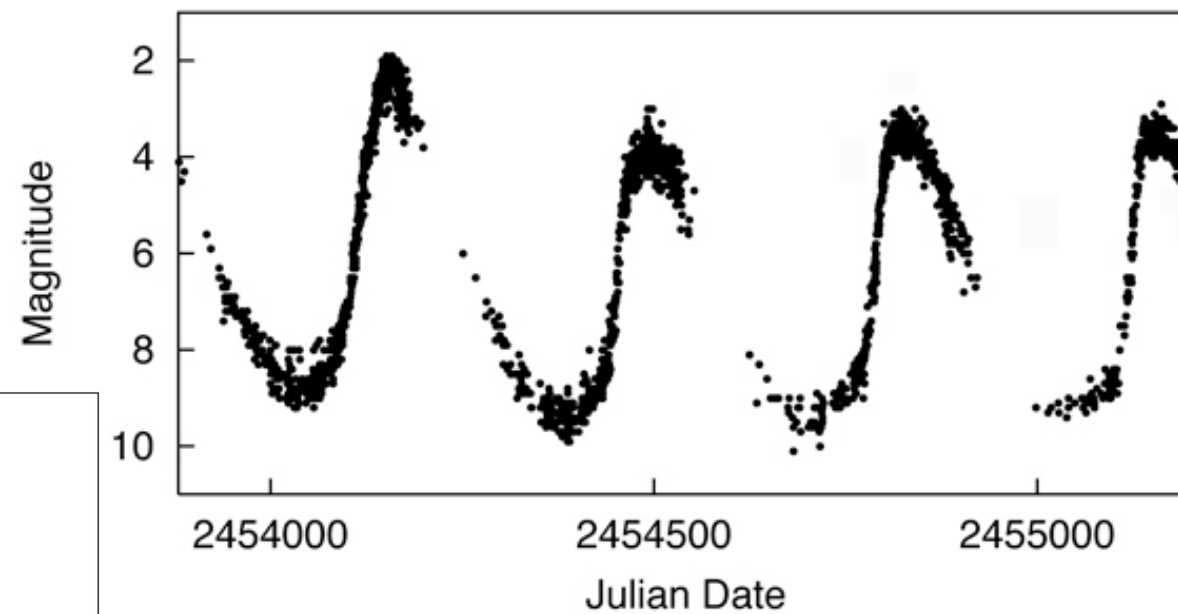
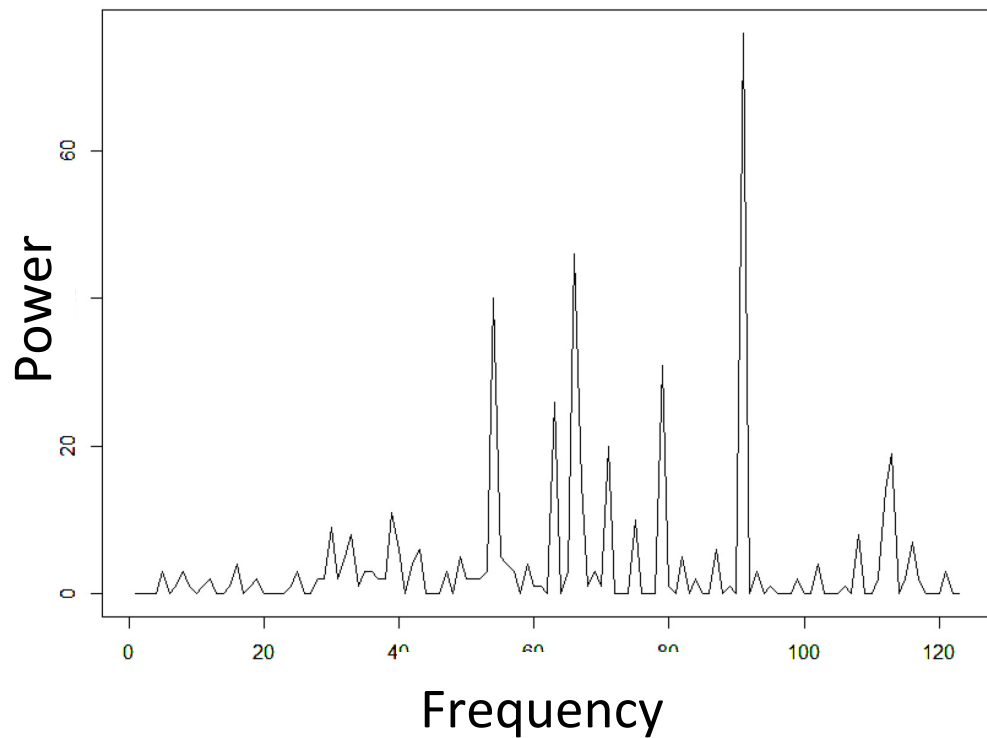
FIGURE 2: Damped harmonic motion with the amplitude decreasing in time illustrating the time asymmetry of a Universe with friction.

$$L = \left(\frac{GM}{2R} \right) \frac{dm}{dt},$$

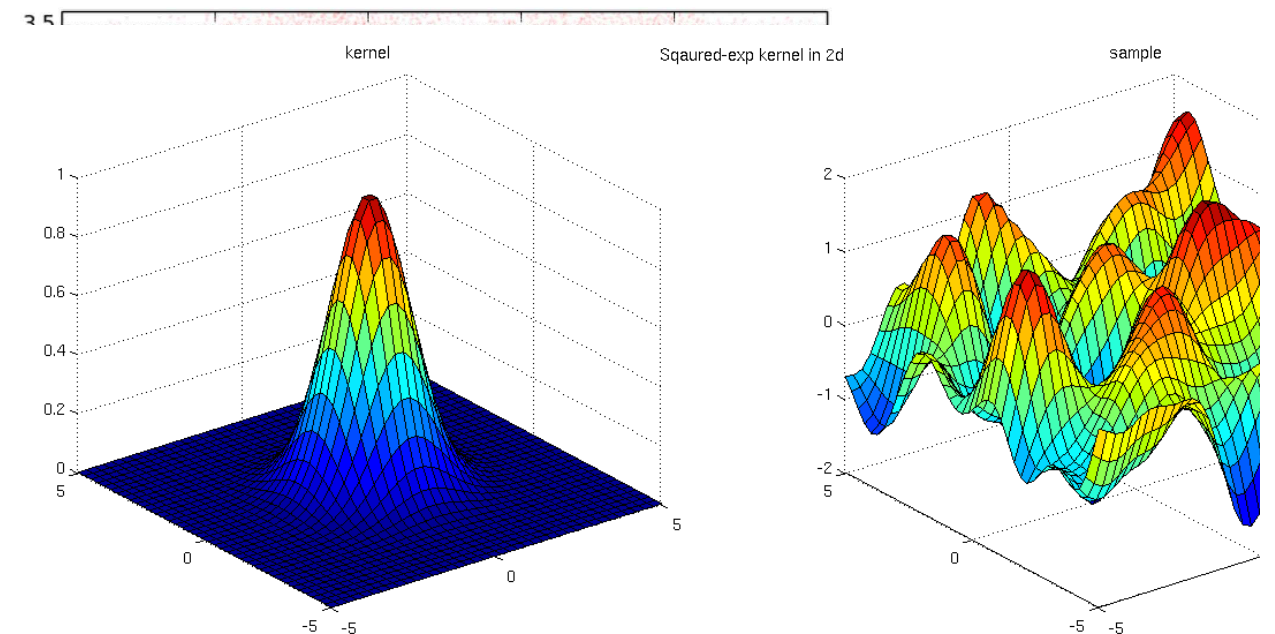
Garofalo 15

Period finding

Early 20th Century:
count the waves

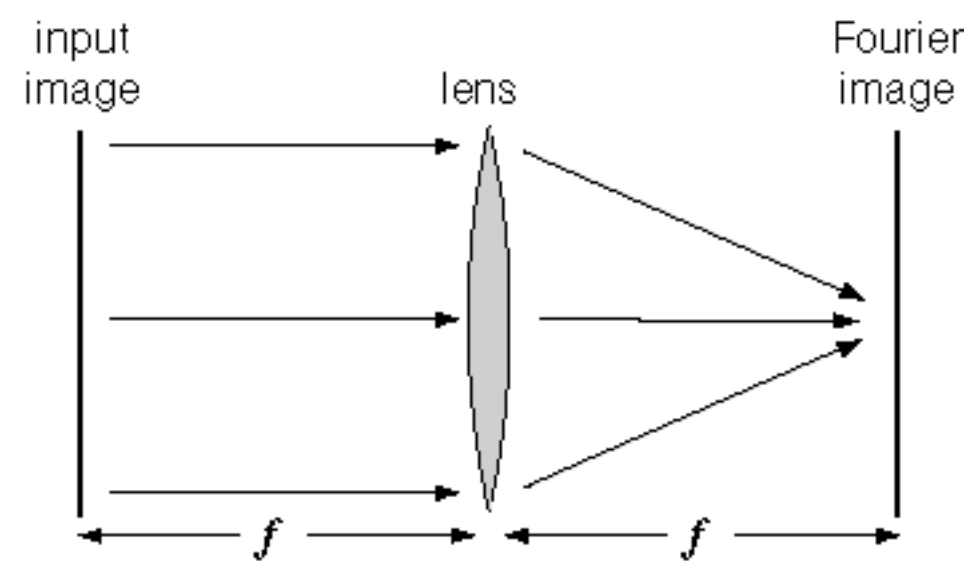
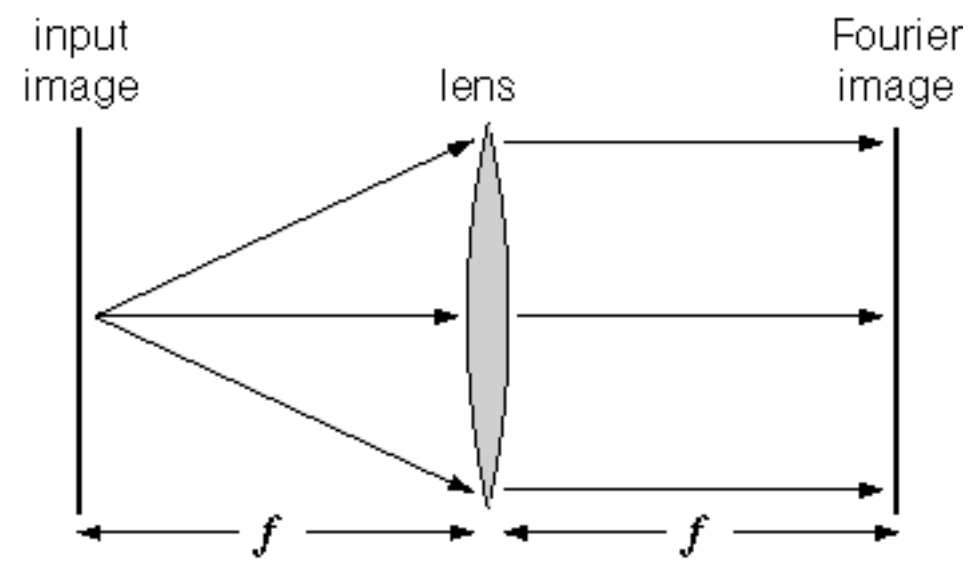
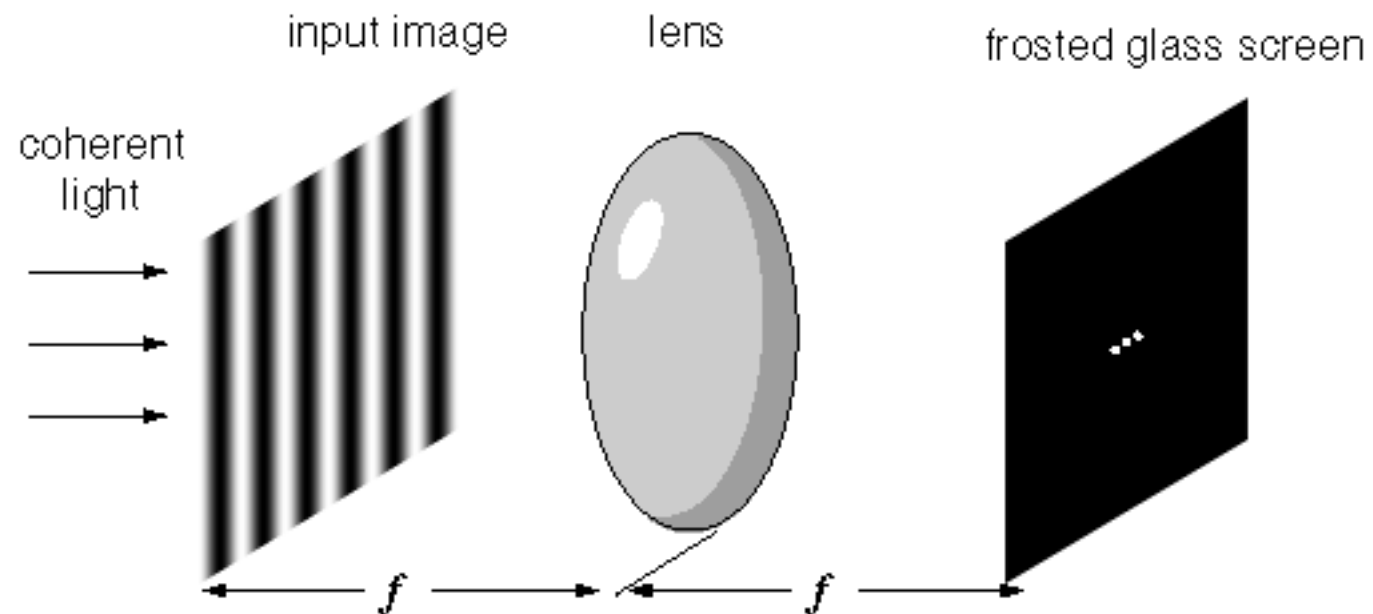


Late 20th Century: periodograms



Early 21st Century:
detailed process modeling

OPTICAL ANALOGY

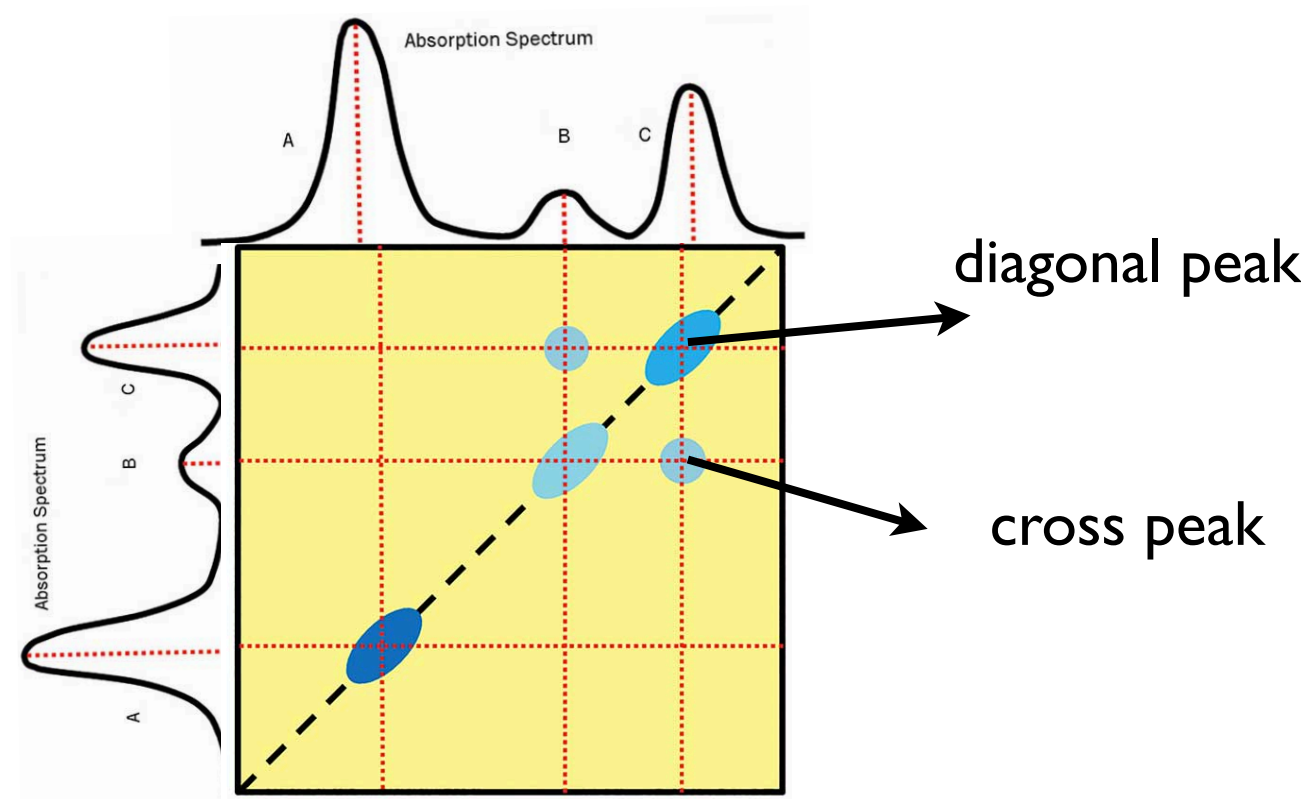


Perturbation
(?stochastic)

System
? or intrinsic
dominant
nonlinear-shift/
catastrophic
regime

$$LC(t) = \text{Dynamical}(t) \times \text{Acceleration}(t) \\ \times \text{Radiation}(t) \times \text{Observation}(t) \text{ [Product]}$$

Hybrid method



Light curves

Table 1. AGN sample for testing periodic variability. Columns are: object name, AGN type, redshift, total period of monitoring programs, the combined light curve, mean sampling of the combined light curve, excess variance of the combined light curves, literature from which combined light curves were compiled.

Object name	Type	z	Period	CLC	Sampling (days)	EV	Reference ^a
3C 390.3	BLRG	0.056	1994-2014	Continuum 5100 Å	11.6	0.1623	1, 2, 3, 4, 5
				H α	34.5	0.1055	
				H β	20.5	0.1099	
			1978-1996	Continuum 1370 Å	64.4	0.1737	6, 7
				Ly α	64.4	0.2539	
				CIV	64.4	0.2167	
Arp 102b	LINER	0.024	1987-2010	Continuum 6200 Å	78.1	0.0080	8, 9
				H α	77.0	0.0245	
				Continuum 5100 Å	73.0	0.0073	8
			1993-2006	H β	60.0	0.0090	8
				Continuum 5100 Å	16.1	0.2847	10,11, 12
				H α	39.6	0.0740	
NGC 4151	Seyfert 1	0.003	1993-2006	H β	19.2	0.1367	
				Continuum 5100 Å	6.9	0.0648	13
				H β	11.2	0.0917	
NGC 5548	Seyfert 1	0.017	1972-2015	Continuum 5100 Å	68.4	0.0357	14
				H β	68.4	0.0049	
				Continuum 4200 Å	114.9	0.0359	
			1990-2014	H γ	114.9	0.0356	

^a (1) Dietrich et al. (1998), (2) Shapovalova et al. (2010a), (3) Dietrich et al. (2012), (4) Sergeev et al. (2011), (5) Afanasiev et al. (2015), (6) Wamsteker et al. (1997), (7) O' Brien et al. (1998), (8) Shapovalova et al. (2013), (9) Sergeev et al. (2000), (10) Kaspi et al. (1996), (11) Shapovalova et al. (2010b), (12) Bon et al. (2012), (13) Bon et al. (2016), (14) Shapovalova et al. (2016).

ARP 102 B

observed:
1987–2010

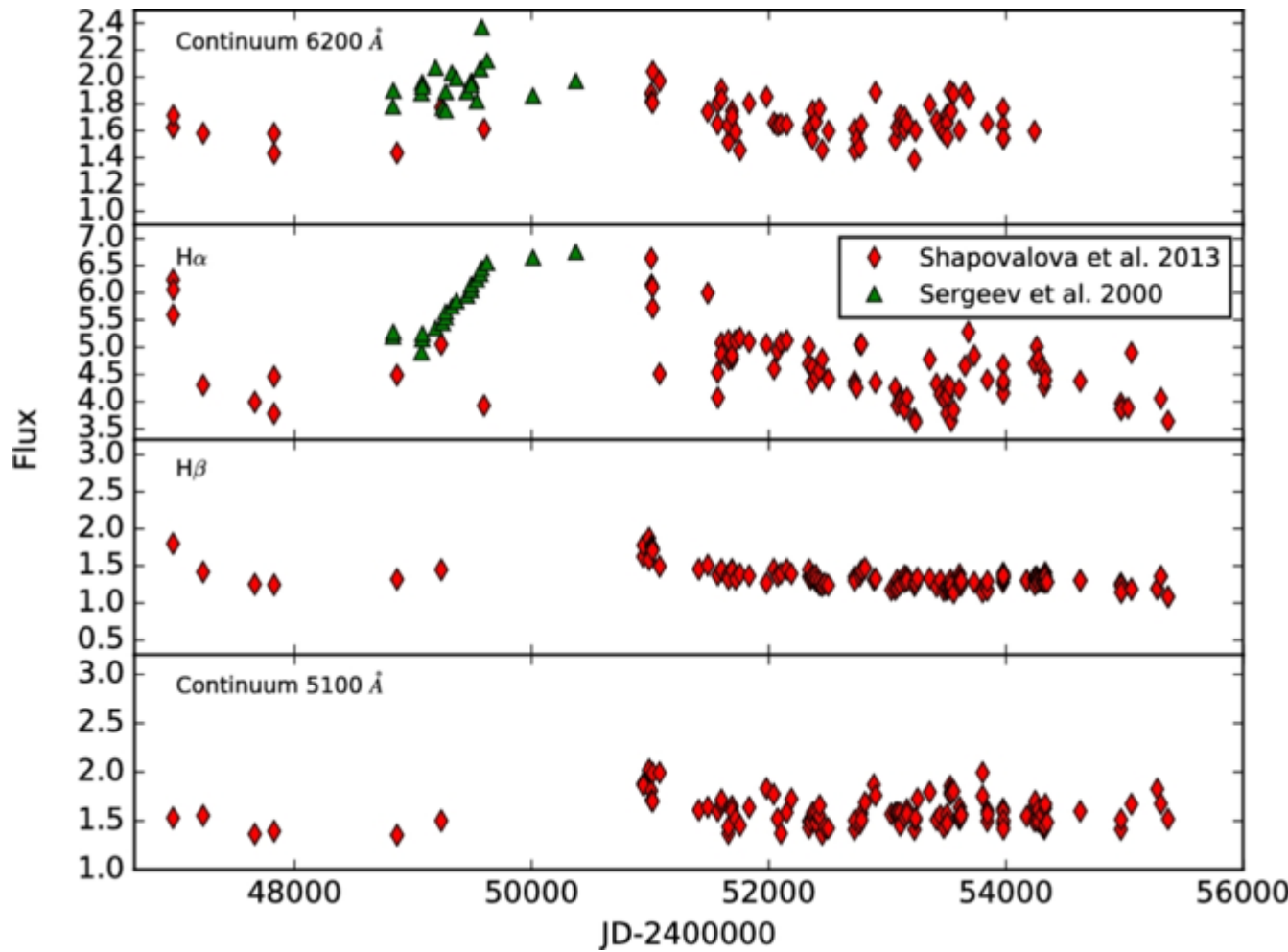
sampling:

78.1 days

77 days

73 days

60 days



3C 390.3

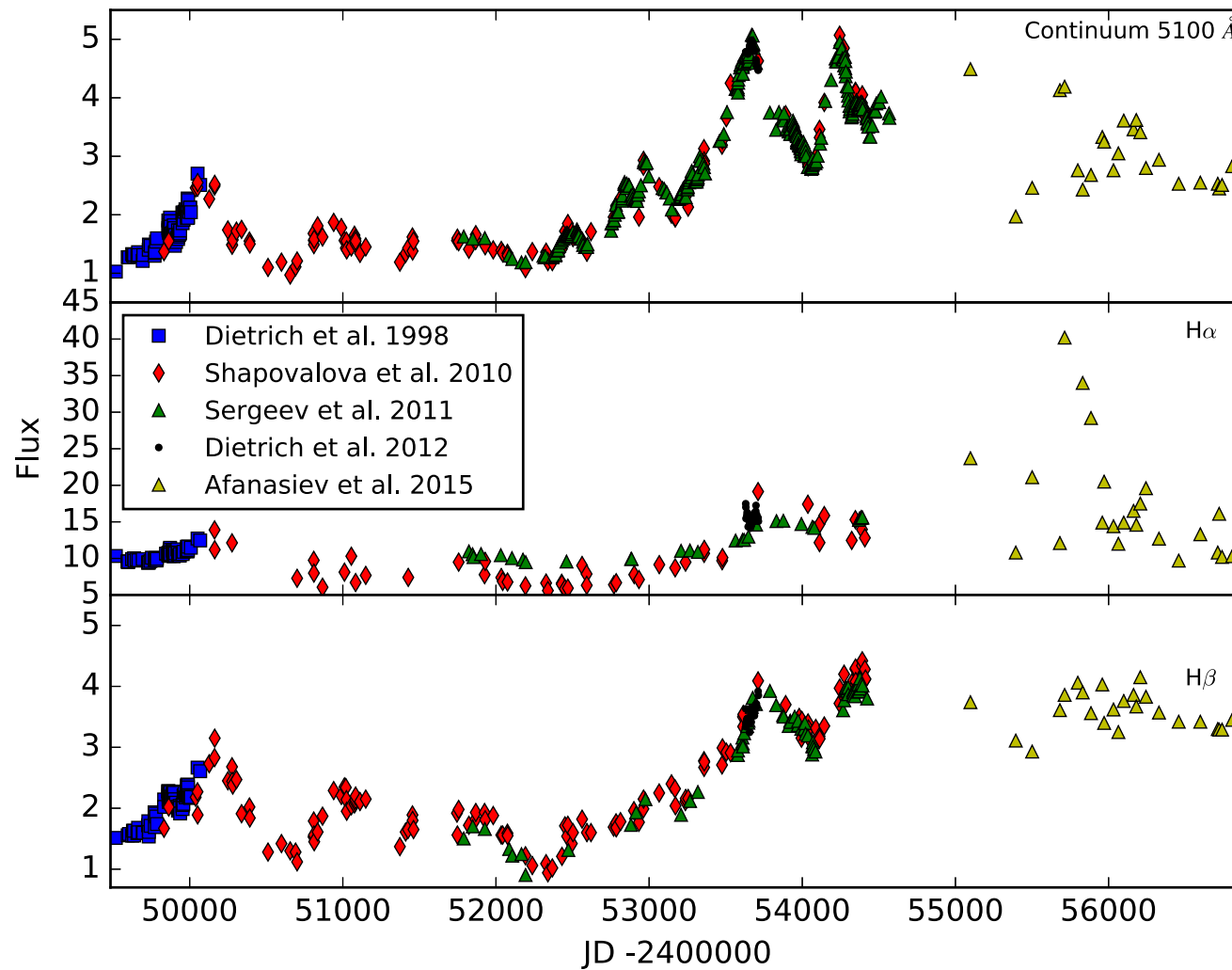
observed:
1994–2014

sampling:

11.6 days

34.5 days

20.5 days



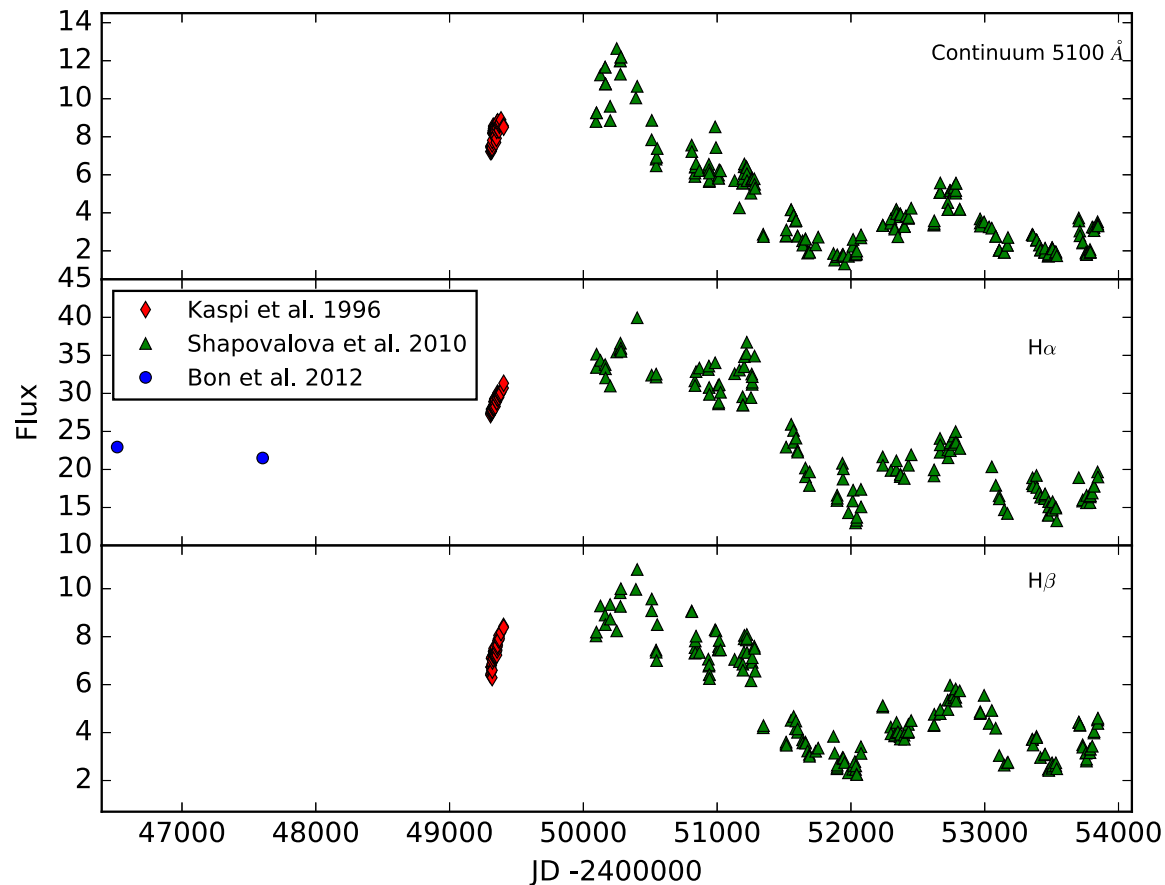
NGC 4151

sampling:

16.1 days

39.6 days

19.2 days



**observed:
1993–2006**

**observed:
1986–2006**

**observed:
1993–2006**

HYBRID METHOD: 3 STEPS

OUGP=Ornstein–Uhlenbeck Gaussian Process

OUGP(raw LC1)=OUGP1

OUGP(raw LC2)=OUGP2

0 STEP:
raw data
preprocessing

$$\text{CWT}(a, b) = \frac{1}{\sqrt{2\pi a}} \int_{-\infty}^{+\infty} x(t) e^{[(t/b)^2/a/2]\beta^2} e^{i\omega(t-b)/a} dt,$$

$$\text{env}(a, b) = \sqrt{\text{Re}\{[\text{CWT}(a, b)]^2\} + \text{Im}\{[\text{CWT}(a, b)]^2\}},$$

I STEP

SpearmanCorrCoeff(env(OUGP1),env(OUGP2)) 2 STEP

time series. The complex Morlet wavelet transform of time series $x(t)$ at an arbitrary scale a and for translational parameter b can be formulated as ([Yang & Tse 2005](#))

$$\text{CWT}(a, b) = \frac{1}{\sqrt{2\pi a}} \int_{-\infty}^{+\infty} x(t) e^{[(t/b)^2/a/2]\beta^2} e^{i\omega(t-b)/a} dt \quad (1)$$

where $i = \sqrt{-1}$, ω is frequency of the wavelet function and β is parameter controlling the wavelet function's shape. Physically, $\text{CWT}(a, b)$ is the energy of $x(t)$ in scale a at time $t = b$. Then the envelope ($\text{env}(a, b)$) of the wavelet coefficients are given by the following metric expression ([Yang & Tse 2005](#))

$$\text{env}(a, b) = \sqrt{\text{Re}[(\text{CWT}(a, b))^2] + \text{Im}[(\text{CWT}(a, b))^2]} \quad (2)$$

where Re, Im stand for the real and the imaginary part of a given CWT.

colors). Since the values of the position parameter b can be continuously varied, and the scaling a can be defined from the minimum (original signal scale) to a maximum chosen by the user, the CWT can be seen as a function of scales a as it is shown in [Grinsted et al. \(2004\)](#). For the Morlet wavelet the period is almost equal to the scale (see [Grinsted et al. 2004](#)). So the x and y axes of the correlation plots depicts scales a , or equivalently, periods. If the same

0 STEP: PREPROCESSING DATA

What is GP

Gaussian distribution

* is a distribution over **vectors**

*specified by mean and a covariance
(vectors) $x \sim G(\mu, \Sigma)$

*the position of the random variables
 x_i plays the role of the index

Gaussian Process

* is a distribution over **functions**

*specified by mean function and a
covariance function $f \sim GP(m, k)$

*the argument x of the random
function $f(x)$ plays the role of the
index

Ornstein–Uhlenbeck Gaussian Process

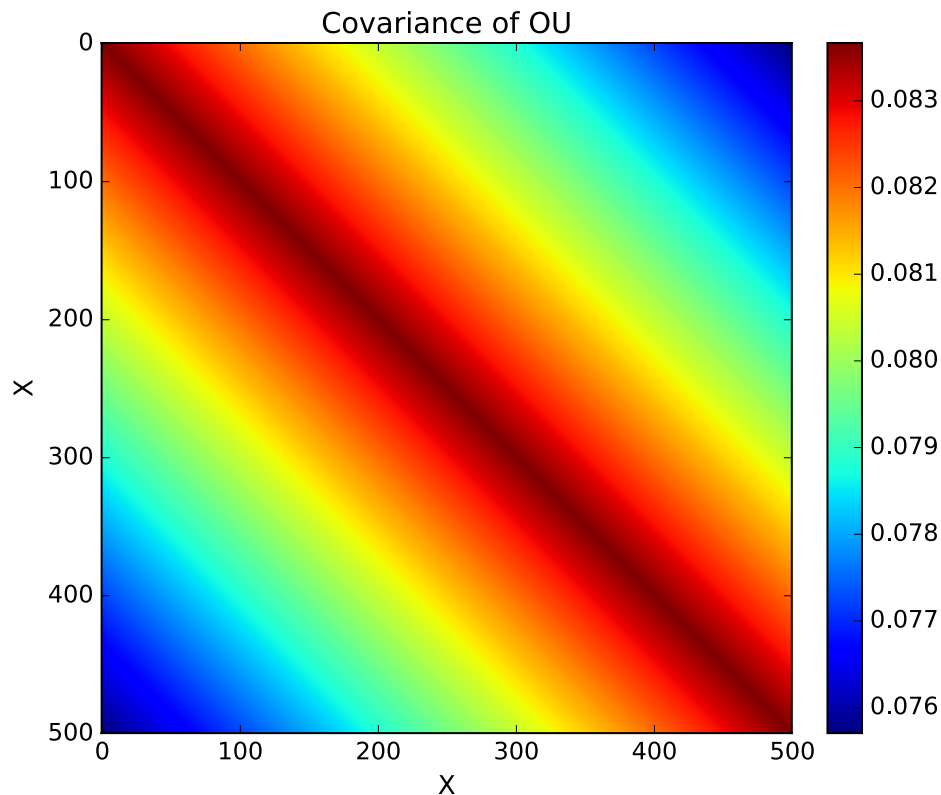
GP is defined by mean function and a covariance function

$f \sim GP(m, K)$, $m \sim 0$

variance

$$K_{OU}(x, x') = \boxed{\sigma^2} \exp\left(-\frac{|x - x'|}{\boxed{l}}\right),$$

length scale



Kovacevic, Popovic, Shapovalova, Ilic, 2017

The simplified version of GPs (namely continuous time first-order autoregressive process (CAR(1))) has been used to model AGN continuum light curves (see Pancoast et al. 2014, and reference therein). These works used Ornstein - Uhlenbeck (OU) covariance function:

$$K_{\text{OU}}(\Delta t) = \frac{\hat{\sigma}^2}{2\alpha_0} \exp^{-\alpha_0 \Delta t}$$

where $\frac{1}{\alpha_0}$ is characteristic time scale, $\hat{\sigma}^2$ is variance of driving noise, and Δt is the time separating two observations (see Kelly et al. 2014). (Note here that this kernel can be written also in the form

$$K_{\text{OU}}(x, x') = \sigma^2 \exp\left(-\frac{|x - x'|}{l}\right),$$

where the parameter σ^2 is the variance and l is the characteristic length scale of the process, i. e. how close two points x and x' have to be to influence each other. The OU process is a stationary GP. Since the information about the underlying nature of AGN light curves is crucial for probing their variability, Kelly et al. (2011), Andrae et al. (2013) and Zu et al. (2013) modeled the light curves as a parameterized stochastic process with composite covariance functions. Following the same direction of investigations, we applied some of stationary and non-stationary composite covariance functions. As they are a linear combination of other simpler covariance functions, we are able to incorporate insight about periodicity, red noise and nonstationarity of underlying processes.

In our research we employed two kind of kernel families: stationary - already mentioned OU precess, the squared exponential (SE):

$$K_{\text{SE}}(\Delta t) = \frac{\hat{\sigma}^2}{2\alpha_0} \exp^{-(\alpha_0 \Delta t)^2},$$

which alternative representation is

$$K_{\text{SE}}(x, x') = \sigma^2 \exp\left(-\frac{\|x - x'\|^2}{2l^2}\right),$$

rational quadratic (RQ)

$$K_{\text{RQ}}(\Delta t) = \frac{\hat{\sigma}^2}{2\alpha_0} \left(1 + \frac{\alpha_0^2 |\Delta t|^2}{\alpha}\right)^{-\alpha}, \text{ with } \alpha = 2;$$

with an alternative form

$$K_{\text{RQ}}(x, x') = \sigma^2 \left(1 + \frac{|x - x'|^2}{\alpha l^2}\right)^{-\alpha} \text{ with } \alpha = 2;$$

non-stationary – the standard periodic kernel (StdPer)

$$K_{\text{StdPer}}(\Delta t) = \frac{\hat{\sigma}^2}{2\alpha_0} \exp\left(-\frac{2 \sin^2\left(\frac{\pi(\Delta t)}{P}\right)}{\left(\frac{1}{\alpha_0}\right)^2}\right)$$

with alternative version

$$K_{\text{StdPer}}(x, x') = \sigma^2 \exp\left(-\frac{2 \sin^2\left(\frac{\pi(x-x')}{P}\right)}{l^2}\right);$$

and Brownian motion (Brw, red noise or Wiener process)

$$K_{\text{Brw}}(\Delta t) = \frac{\hat{\sigma}^2}{2\alpha_0} \min(\Delta t),$$

which alternative form is

$$K_{\text{Brw}}(x, x') = \sigma^2 \min(x, x').$$

that OU models can be a degenerate descriptors. A CARMA models might serve better for this purpose, particularly as the red noise terms in them can produce quasi-periodicities which are missing from simple OU

models. For the purpose of CARMA modeling we used Brandon Kelly carma_pack Python package available on https://github.com/brandonckelly/carma_pack. CARMA models lightcurve as sum of (deterministic) autoregression plus (random) stochastic noise. The CARMA model order input is optional. We automatically choose the CARMA order (parameters (p,q)) by minimizing the AIC (Akaike Information Criterion). Also, the residuals from the one-step-ahead predictions standardized by their standard deviation were uncorrelated. Random light curves were sampled with built in functions in GPy and farm_pack packages.

We recalculated periods of each real and simulated curve (see Figure 2) by means of Bayesian formalism for the generalized LS periodogram (BGLS Mortier et al. 2015), which gives the probability of signal's existence in the data. It can be seen that powers of BGLS peaks of OU and CARMA 'red noise' curves are asymptotically close to each other as well as to the continua 4200 Å 5100 Å and the H γ line (Figure 2).

Due to this fact we will consider as base red noise model OU. Also, in our calculations will be included models given by Eq. 3 and

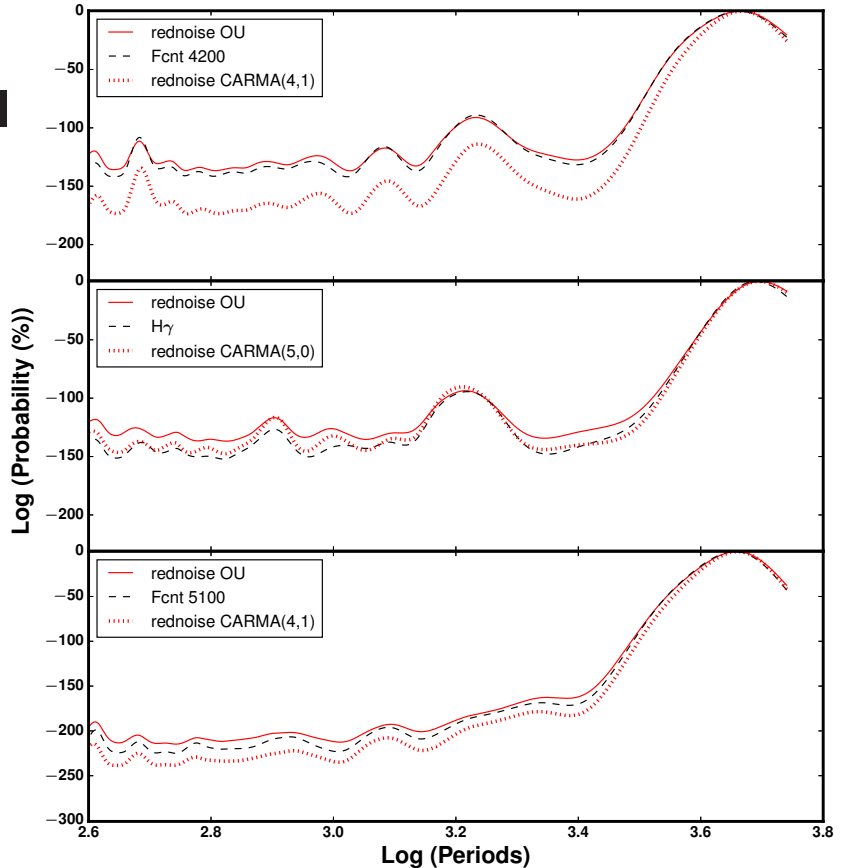
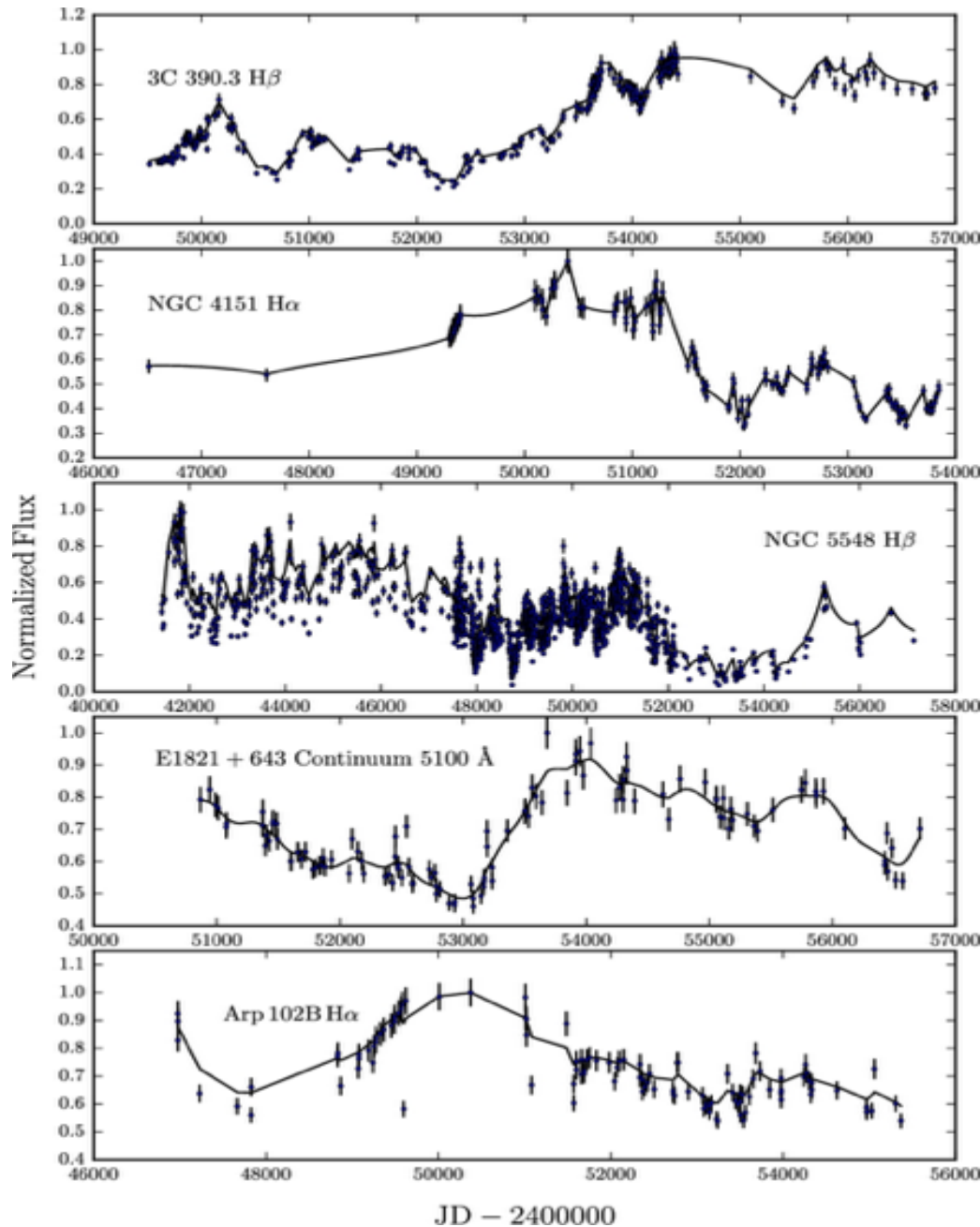


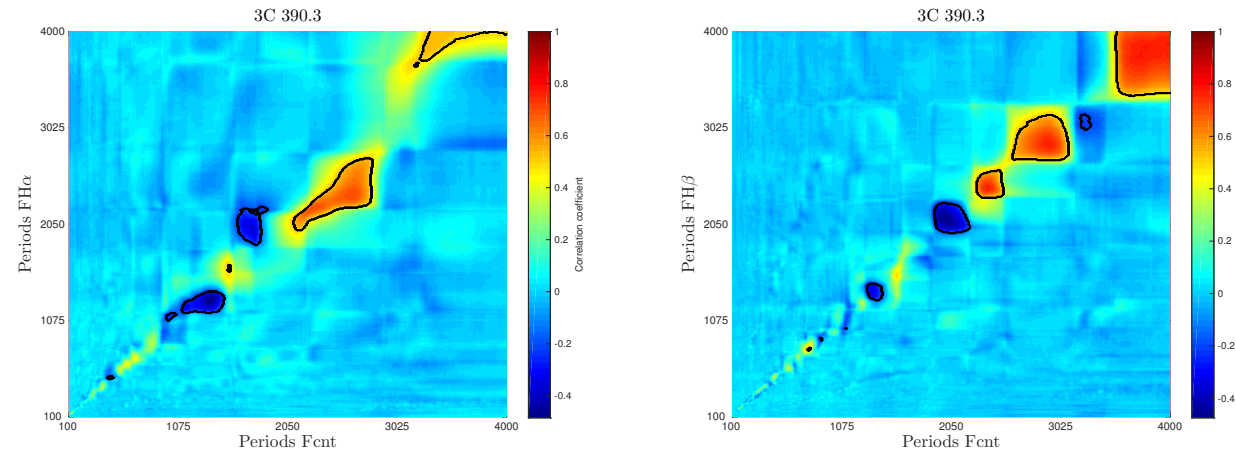
Fig. 2 Bayesian periodograms of the simulated 'red noise' and real light curves on a logscale.

0 STEP: RAW DATA PREPROCESSING

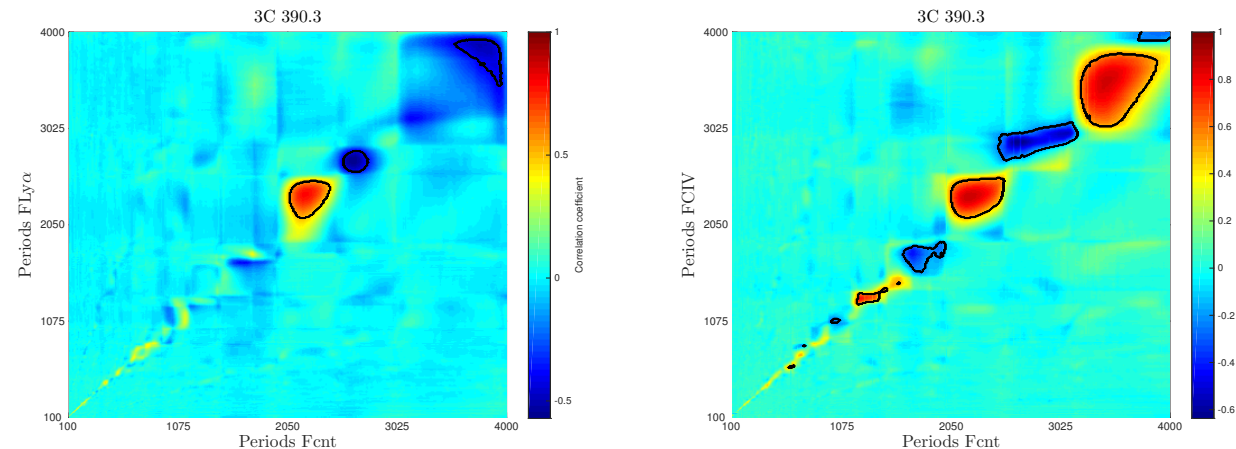


Examples of the comparison between the GP posterior mean (solid line) and observed light curves (dots) for the five objects.

1 STEP: RESULTS

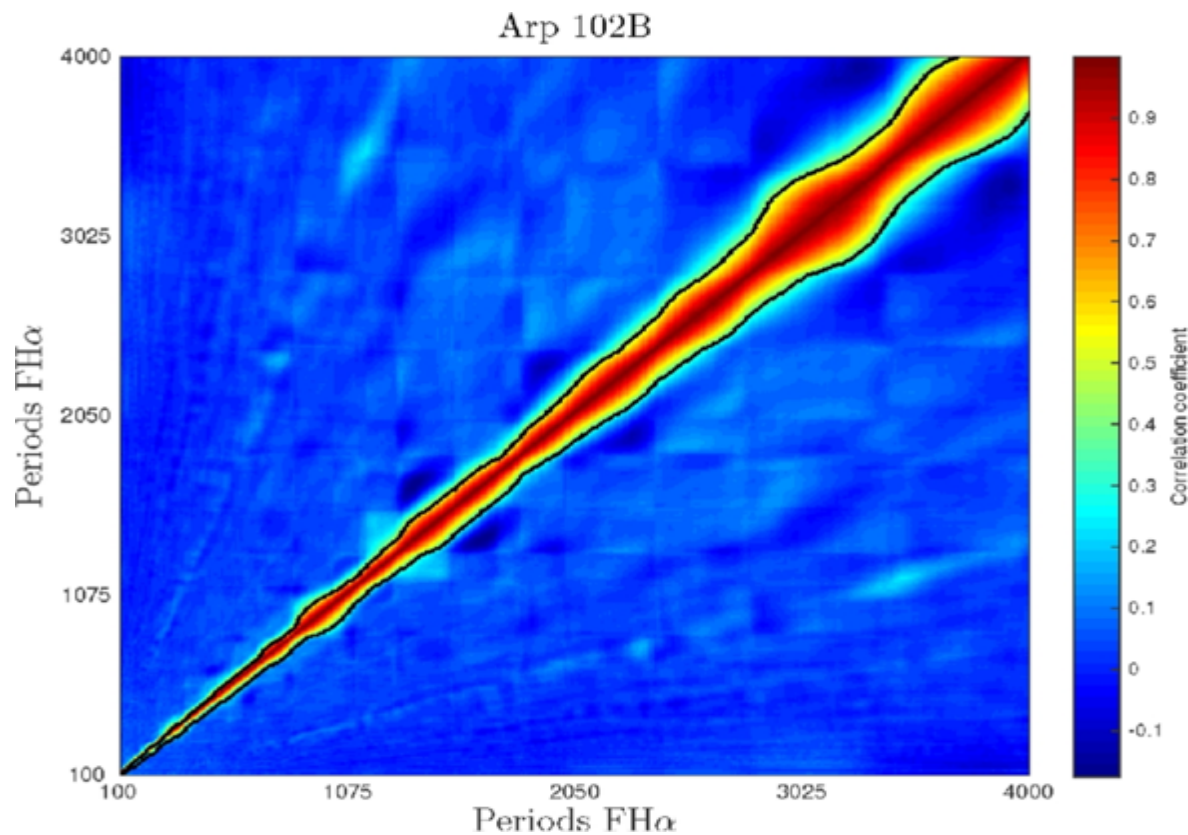


3C 390.3



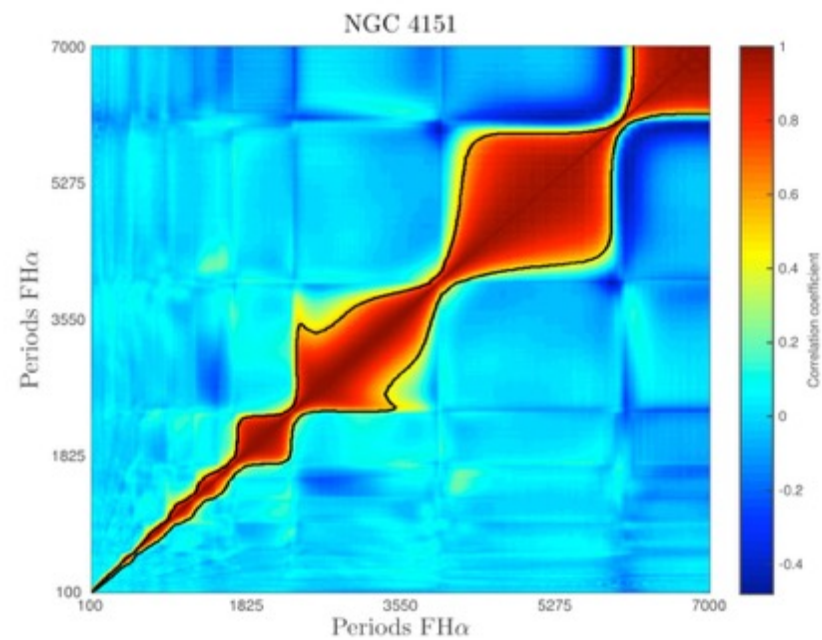
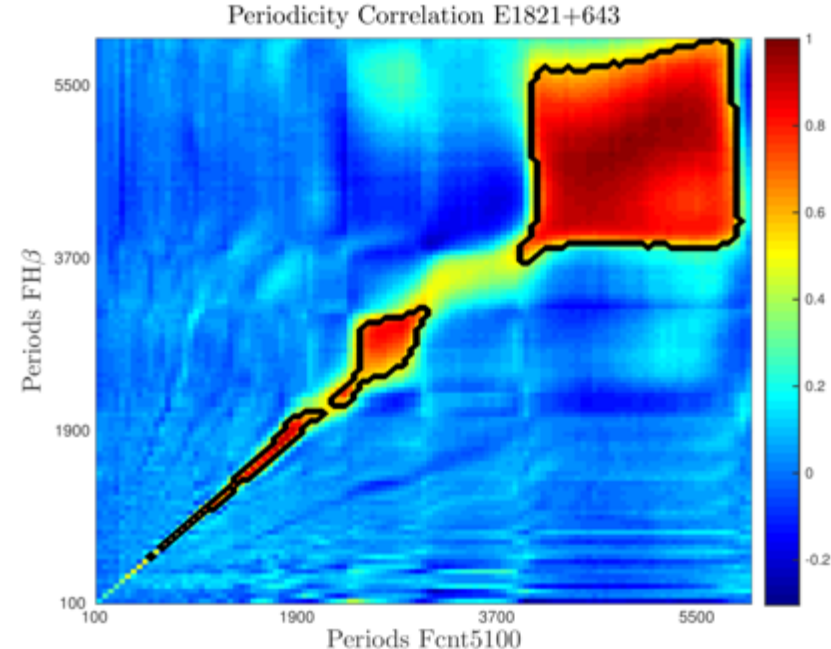
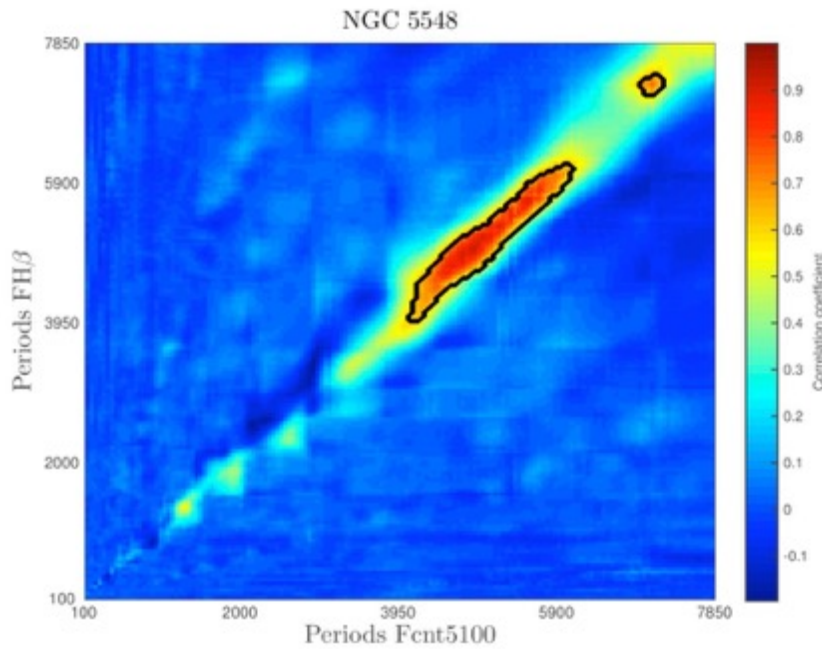
Object name	CLC1	CLC2	$P \pm \Delta P$ [yr]	r	95%CI	p
3C 390.3	Continuum 5100 Å	H α	9.5 ± 0.3	0.5	(0.49,0.51)	< 0.00001
			7.2 ± 1.2	0.69	(0.68,0.7)	< 0.00001
			$6.3 + 0.9$	0.68	(0.67,0.69)	< 0.00001
			4.0 ± 0.04	-0.47	(-0.48,-0.45)	< 0.00001
			5.44 ± 0.1	-0.35	(-0.37,-0.33)	< 0.00001
	H β		10.11 ± 0.1	0.77	(0.76,0.78)	< 0.00001
			7.67 ± 0.02	0.71	(0.7,0.72)	< 0.00001
			$6.42 + 1.6$	0.75	(0.74,0.76)	< 0.00001
			5.43 ± 0.8	-0.47	(-0.48,-0.45)	< 0.00001
	Continuum 1370 Å	Lya	3.6 ± 0.4	-0.33	(-0.35,-0.31)	< 0.00001
			10.34 ± 0.1	-0.47	(-0.49,-0.45)	< 0.00001
			7.1 ± 0.02	-0.53	(-0.54,-0.51)	< 0.00001
			6.25 ± 1.42	0.77	(0.76,0.78)	< 0.00001
		CIV	9.42 ± 0.02	0.85	(0.84,0.86)	< 0.00001
			7.84 ± 0.02	-0.6	(-0.61,-0.59)	< 0.00001
			6.4 ± 1.22	0.85	(0.84,0.86)	< 0.00001
			4.68 ± 0.7	-0.42	(-0.44,-0.40)	< 0.00001
			3.4 ± 0.4	0.75	(0.74,0.76)	< 0.00001

ARP 102B



Note the prominent stationarity of the diagonal correlation line and the absence of correlation clusters.

Object name	CLC1	CLC2	$P \pm \Delta P$ (yr)	r	95% CI	p
Arp 102B	Continuum 6200 Å	H α	—	—	—	—
	Continuum 5100 Å	H β	—	—	—	—



NGC 4151	Continuum 5100 Å	H α	13.76 ± 3.73	0.96	(0.956,0.962)	< 0.00001
			8.33 ± 2.33	0.97	(0.968,0.972)	< 0.00001
			5.44 ± 1.29	0.98	(0.978,0.981)	< 0.00001
NGC 5548	Continuum 5100 Å	H β	13.3 ± 2.26	0.87	(0.867,0.873)	< 0.00001
E1821+643	Continuum 5100 Å	H β	12.76 ± 5.6	0.98	(0.979,0.981)	< 0.00001
			6.93 ± 1.99	0.80	(0.792,0.808)	< 0.00001
			4.75 ± 0.79	0.80	(0.792,0.808)	< 0.00001
	Continuum 4200 Å	H γ	12.36 ± 6.1	0.99	(0.989,0.991)	< 0.00001
			6.52 ± 3.26	0.91	(0.906,0.914)	< 0.00001
			4.34 ± 0.74	0.94	(0.937,0.943)	< 0.00001

CHECKING RESULTS ON 3 LEVELS

- **1L**>non linear least square fitting of multisinusoidal models to the observed light curves

$$y = \sum_{i=1}^n c_i \sin\left(\frac{2\pi t}{p_i} + \phi_i\right) + B.$$

- **2L**>comparison of dynamics of observed light curves and time-series models

MODEL1 (**linearly** coupled oscillators of 2 units)

$$U_a(t) = A(t) \sin(2\pi f_a t + \phi) + cp_{b \rightarrow a} \quad (3)$$

$$\times B(t) \sin(2\pi f_b t + 2\pi f_b \tau) + W(t) \quad (4)$$

$$U_b(t) = B(t) \sin(2\pi f_b t) + cp_{a \rightarrow b} \quad (5)$$

$$\times A(t) \sin(2\pi f_a t + 2\pi f_a \tau + \phi) + W(t). \quad (6)$$

- MODEL3 (**nonlinearly** coupled oscillators of 3 units)

$$U_a(t) = A(t) \sin(2\pi f_a t + \phi) + cp_{b \rightarrow a} \quad (7)$$

$$\times B(t) \sin(2\pi f_b t + 2\pi f_b \tau) + cp_{c \rightarrow a} \quad (8)$$

$$\times C(t) \sin(2\pi f_c t + 2\pi f_c \tau_1) + W(t) \quad (9)$$

$$U_c(t) = B(t) \sin(2\pi f_b t) + C(t) \sin(2\pi f_c t) + cp_{a \rightarrow b} \quad (10)$$

$$\times A(t) \sin(2\pi f_a t + 2\pi f_a \tau + \phi) + cp_{a \rightarrow c} \quad (11)$$

$$\times A(t) \sin(2\pi f_a t + 2\pi f_a \tau_1 + \phi_1) + W(t). \quad (12)$$

$$U_a(t) = A(t) \sin(2\pi f_a t + \phi) + cp_{b \rightarrow a} \quad (16)$$

$$\times B(t) \sin(2\pi f_b t + 2\pi f_b \tau) + W(t) \quad (17)$$

$$U_b(t) = B(t) \sin(2\pi f_b t) + cp_{a \rightarrow b} \quad (18)$$

$$\times U_a(t)^2 + W(t). \quad (19)$$

3L of checking: HILBERT TRANSFORM

$$H[x(t)] = \frac{1}{\pi} P \int_{-\infty}^{\infty} \frac{x(\tau)}{t-\tau} d\tau$$

$$z(t) = a(t)e^{j\theta(t)}$$

$$a(t) = \sqrt{x^2(t) + \{H[x(t)]\}^2}, \text{ and } \theta(t) = \arctan\left(\frac{H[x(t)]}{x(t)}\right) \quad (3.3)$$

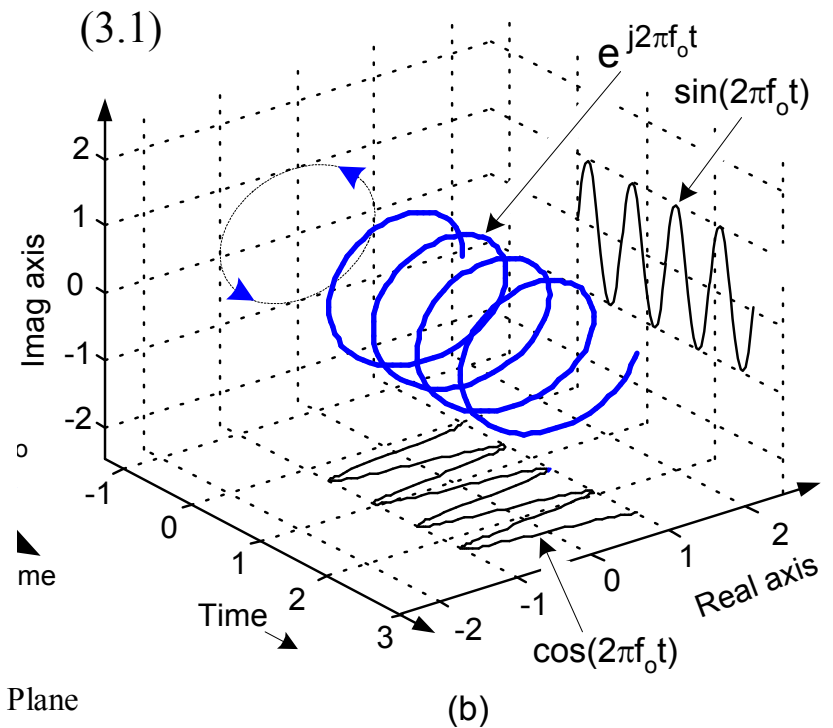
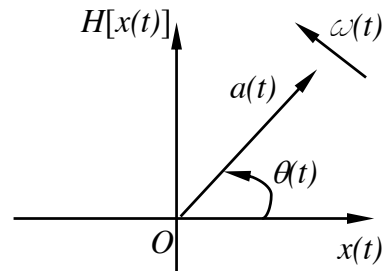
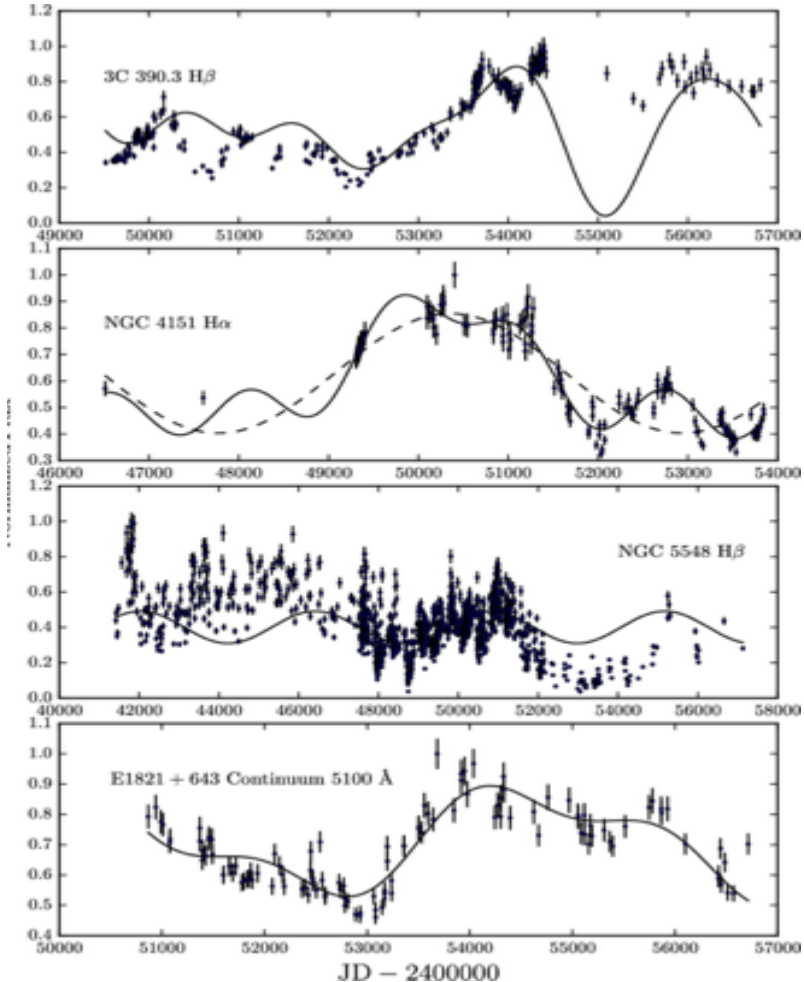


Figure 3.1. Instantaneous Amplitude, Phase Angle and Frequency in Complex Plane

the page, to show the spiral path of the phasor. Figure 6(b) shows a continuous version of just the tip of the $e^{j2\pi f_0 t}$ phasor. That $e^{j2\pi f_0 t}$ complex number, or if you wish, the phasor's tip, follows corkscrew path spiraling along, and centered about, the time axis. The real and imaginary parts of $e^{j2\pi f_0 t}$ are shown as the sine and cosine projections in Figure 6(b).

IL of CHECKING:multisinusiod fitting



Estimated parameters of sinusoidal best-fitting of normalized observed light curves.

Object name	LC	c_i	p_i (d)	ϕ_i (rad)	B	r	χ^2
3C 390.3	$H\beta$	0.11 ± 0.02	3760 ± 7	6.02 ± 0.01	0.52 ± 0.01	0.81	4.748
		0.05 ± 0.03	2743 ± 15	5.51 ± 0.03			
		0.29 ± 0.04	2300 ± 2	5.47 ± 0.03			
		0.17 ± 0.03	2000 ± 2	0.17 ± 0.005			
		0.08 ± 0.01	1322 ± 1	-5.24 ± 0.1			
NGC 4151	$H\alpha$	0.22 ± 0.01	5580 ± 435	1.52 ± 4.34	0.63 ± 0.02	0.96	0.381
		-0.07 ± 0.02	2730 ± 422	-4.20 ± 5.63			
		-0.08 ± 0.01	1534 ± 28	-4.02 ± 3.82			
NGC 5548	$H\alpha$	-0.23 ± 0.01	5165 ± 3	-	0.63 ± 0.01	0.87	1.275
		-0.10 ± 0.01	4378 ± 70	-5.35 ± 1.12	0.40 ± 0.004	0.40	32.804
E1821 + 643	Continuum 5100 Å	0.16 ± 0.001	4511 ± 1	0.02 ± 0.005	0.71 ± 0.0	0.87	0.449
		0.50 ± 0.0002	2529 ± 0.005	1.57 ± 0.03			
		0.07 ± 0.005	1977 ± 0.1	1.10 ± 0.002			

$$y = \sum_{i=1}^n c_i \sin\left(\frac{2\pi t}{p_i} + \phi_i\right) + B$$

2L of CHECKING: simulations of coupled oscillators

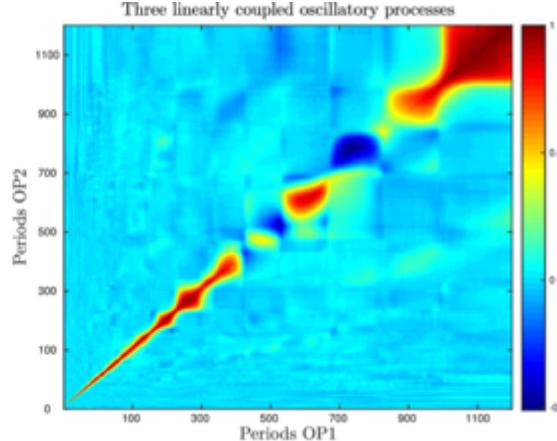
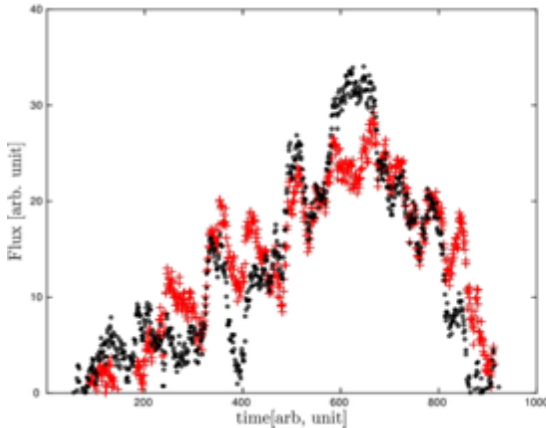
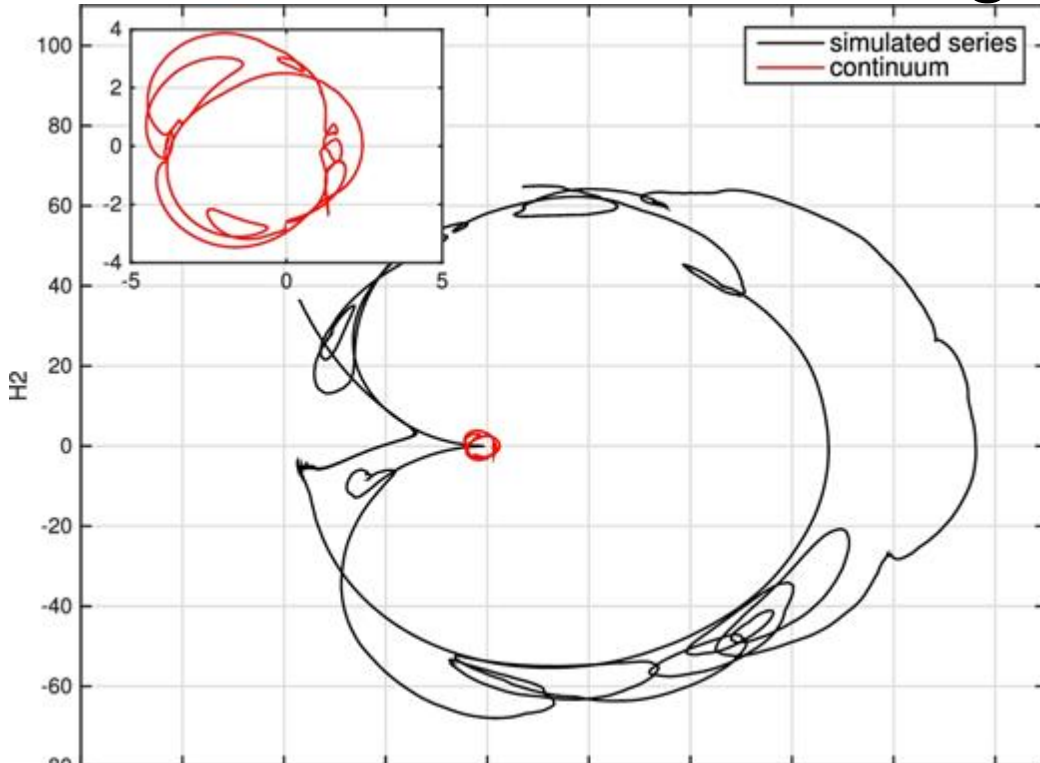


Figure 12. Simulation of bidirectional coupled three oscillators network for the case of 3C 390.3. Left: Random realization of Eq. (4) form two time series (black is $U_a = OP1$, and red is $U_c = OP2$) of amplitudes $A = 1.954$, $B = 1.729$, $C = 2.357$, phase $\phi = \phi_1 = 2.359$ rad coupling strengths $cp_{a \rightarrow b} = 0.7$, $cp_{a \rightarrow c} = 0.5$, $cp_{b \rightarrow a} = 0.2$, $cp_{c \rightarrow a} = 0.3$, frequencies $f_a = \frac{1}{1000}$, $f_b = \frac{1}{300}$, $f_c = \frac{1}{100}$, and time delay of 100 arbitrary chosen time unites. Right: corresponding 2D correlation map, which clearly shows three clusters related to fundamental periods as well as clusters of negative correlation.

Simulation of bidirectional coupled three-oscillator network for the case of 3C 390.3.

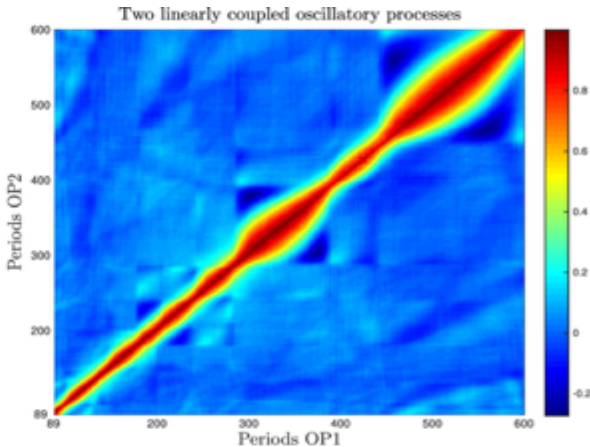
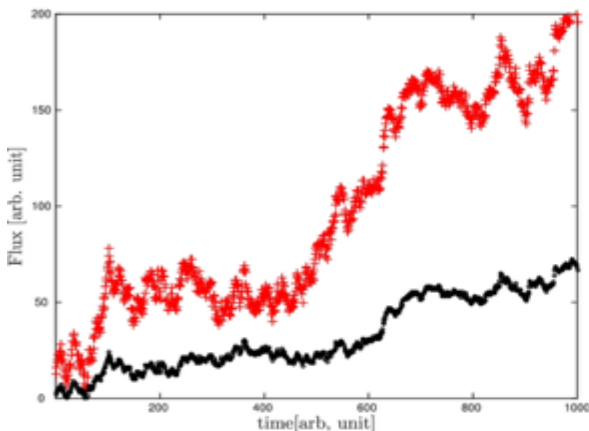
$$\begin{aligned}
 U_a(t) &= A(t) \cdot \sin(2\pi f_a t + \phi) + cp_{b \rightarrow a} \cdot \\
 &\quad B(t) \cdot \sin(2\pi f_b t + 2\pi f_b \tau) + cp_{c \rightarrow a} \cdot \\
 &\quad C(t) \cdot \sin(2\pi f_c t + 2\pi f_c \tau_1) + W(t) \\
 U_c(t) &= B(t) \cdot \sin(2\pi f_b t) + C(t) \cdot \sin(2\pi f_c t) + cp_{a \rightarrow b} \cdot \\
 &\quad A(t) \cdot \sin(2\pi f_a t + 2\pi f_a \tau + \phi) + cp_{a \rightarrow c} \cdot \\
 &\quad A(t) \cdot \sin(2\pi f_a t + 2\pi f_a \tau_1 + \phi_1) + W(t)
 \end{aligned}$$

3L of checking: Hilbert transform



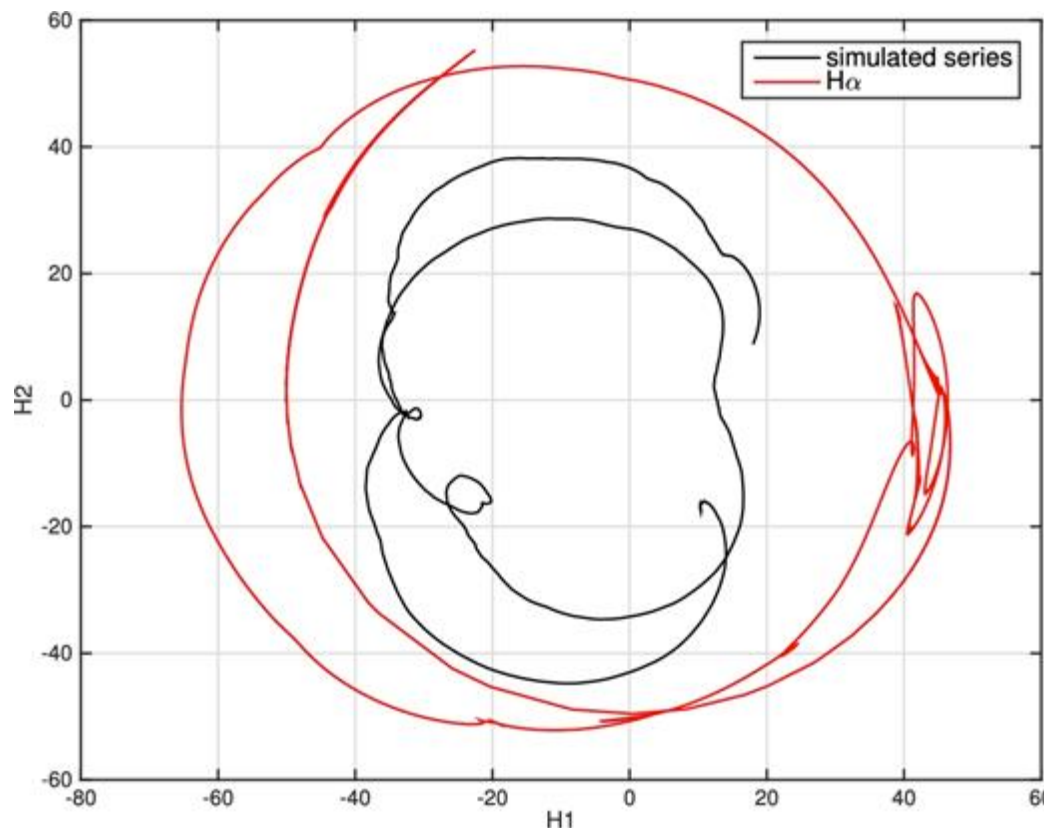
Comparison of the phase trajectories between the continuum of 3C 390.3 and simulated curve OP1 from the oscillatory network model

$$y^H(t) = \frac{1}{\pi} PV \int_{-\infty}^{\infty} \frac{y(\tau)}{t - \tau} d\tau$$



ARP 102B

Simulation of two bidirectional coupled oscillators for the case of Arp 102B. Left: random realization of equation from two time series (black is $U_a = OP1$ and red is $U_b = OP2$) of amplitudes $A = 5.29$, $B = 1.99$, phase $\phi = 0.4174$ rad, coupling strengths $c_{pa \rightarrow b} = 0.4$, $c_{pb \rightarrow a} = 0.2$, time delay is 100 and periods are 500 and 300 arbitrarily chosen time units. Right: corresponding 2D correlation map.



Both curves are similar and non-closed, indicating either weak coupling or the absence of periodicity. They appear to intersect themselves due to projection on to 2D phase space.

$$\begin{aligned} U_a(t) &= A(t) \cdot \sin(2\pi f_a t + \phi) + c p_{b \rightarrow a} \cdot \\ &\quad B(t) \cdot \sin(2\pi f_b t + 2\pi f_b \tau) + W(t) \\ U_b(t) &= B(t) \cdot \sin(2\pi f_b t) + c p_{a \rightarrow b} \cdot \\ &\quad A(t) \cdot \sin(2\pi f_a t + 2\pi f_a \tau + \phi) + W(t) \end{aligned}$$

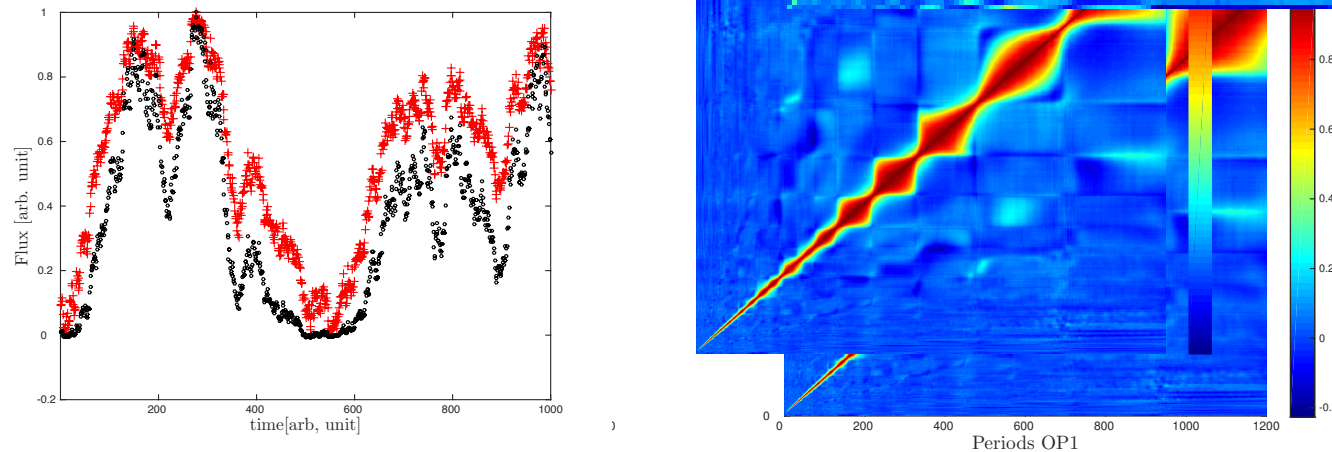


Figure 16. Simulation of two bidirectional coupled oscillators for the case of NGC 4151. Left: Random realization of Eq. (8) form two time series (black is $U_a = OP1$, and red is $U_b = OP2$) of amplitudes $A = 6.09$, $B = 1.04$, phase $\phi = 2.2 \text{ rad}$, coupling strengths $cp_{a \rightarrow b} = 0.7$, $cp_{b \rightarrow a} = 0.6$, periods are 500, 300 and time delay is 100 arbitrarily chosen time units. Note the similarity of sharpness of this signal 'bursts' with features in the observed light curves. Right: corresponding 2D correlation map .

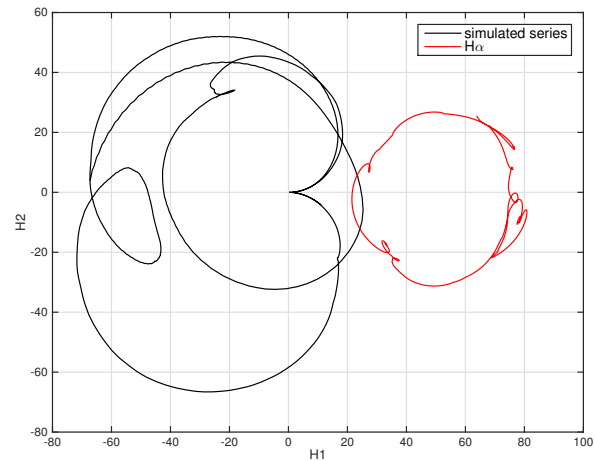
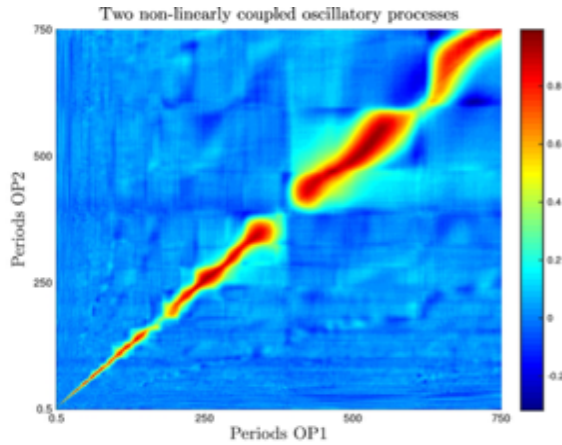
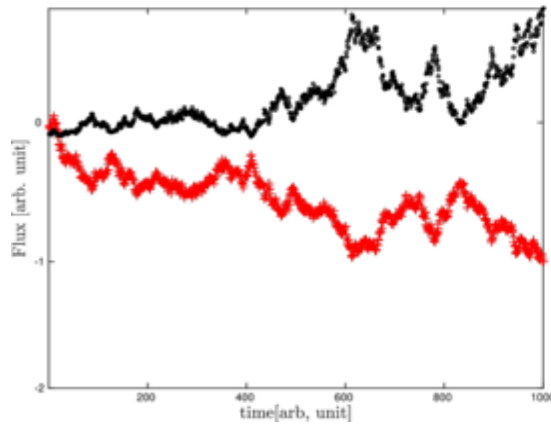


Figure 17. As in Fig. 13 but for the H α line of NGC 4151 and simulated OP1 curve described by Eq. (8) with parameter values as in (see Fig. 16). Note that phase curve of H α line is shifted by + 50 units on x axis for a better view.

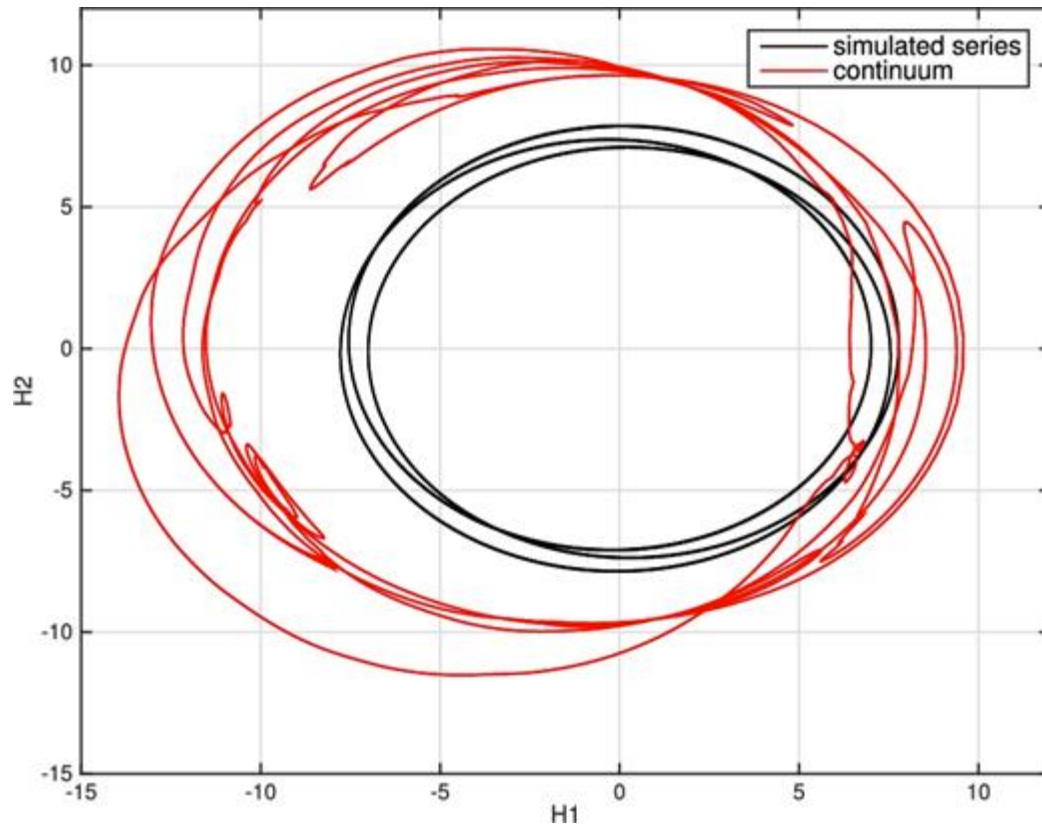
$$\begin{aligned} U_a(t) &= A(t) \cdot \sin(2\pi f_a t + \phi) + cp_{b \rightarrow a} \cdot \\ &\quad B(t) \cdot \sin(2\pi f_b t + 2\pi f_b \tau) + W(t) \\ U_b(t) &= B(t) \cdot \sin(2\pi f_b t) + cp_{a \rightarrow b} \cdot \\ &\quad U_a(t)^2 + W(t) \end{aligned} \quad (8)$$

where the non-linear coupling is introduced by squared term $U_a(t)^2$. Simulated curves consists of sum and multiple of base sinus signals of periods of 500 and 300 arbitrary chosen time units. As a consequence, periods of $2 * 500$, $2 * 300$, 500, 300 are accompanied with an interference patterns $500 + 300$, $500 - 300$ (right plot in Fig. 16). Comparing this scenario with autocorrelation of periods in H α (see Fig. 7), the largest period of 13.76 yr can be interpreted as interference pattern (i.e. sum) of two smaller periods of 5.44 and 8.33 yr.



NGC 5548

Simulation of two bidirectional coupled oscillators for the case of NGC 5548. Left: random realization of equation (19) from two time series (black is $U_a = OP1$ and red is $U_b = OP2$) of amplitudes $A = 5.92$, $B = 1.27$, phases $\phi = 2.65$ rad, coupling strengths $c_{pa \rightarrow b} = 0.7$, $c_{pb \rightarrow a} = 0.2$, periods 500 and 300 and time delay is 100 arbitrarily chosen time units



Note the chaotic-like appearance of both curves.

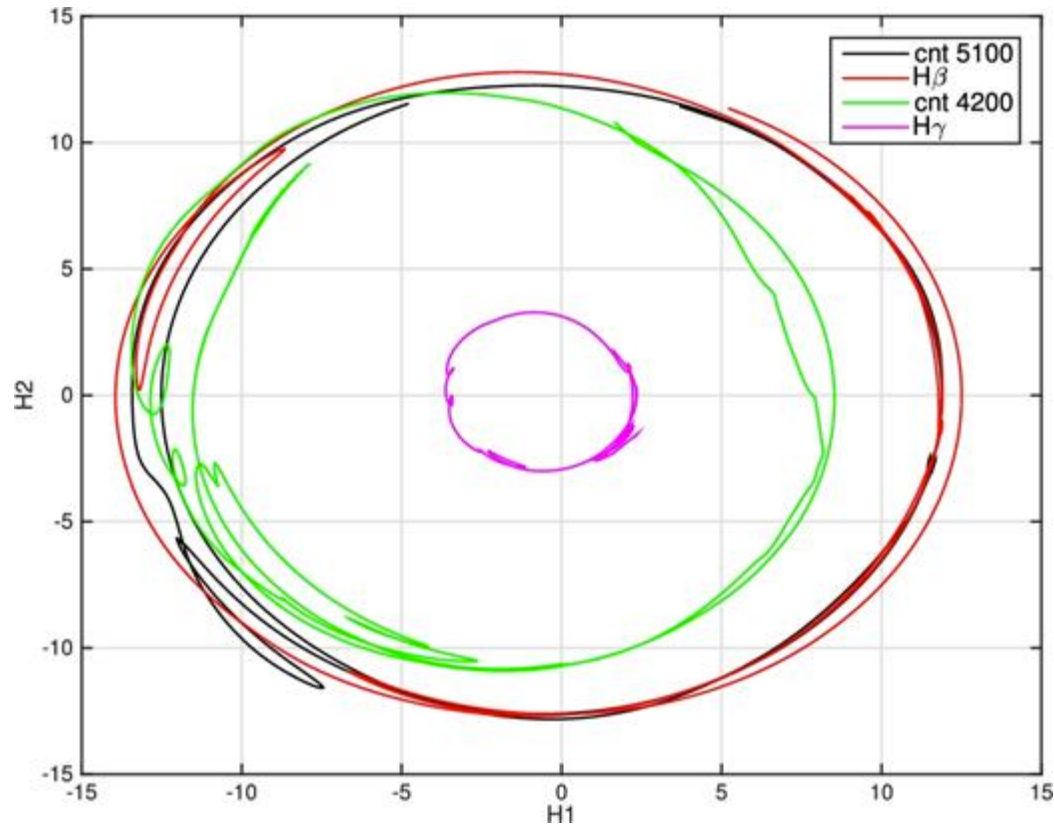
$$U_a(t) = A(t) \sin(2\pi f_a t + \phi) + c_{pb \rightarrow a} U_b(t) \quad (16)$$

$$\times B(t) \sin(2\pi f_b t + 2\pi f_b \tau) + W(t) \quad (17)$$

$$U_b(t) = B(t) \sin(2\pi f_b t) + c_{pa \rightarrow b} U_a(t)^2 + W(t) \quad (18)$$

$$\times U_a(t)^2 + W(t). \quad (19)$$

NGC E1821+643



Its 2D correlation maps are similar to the case of NGC 4151. Particularly, if we look at phase portraits of the light curves normal limit cycles are observed in the dynamics of E1821 + 643. They are similar to the phase portrait of regular sinusoids. We note the presence of two smaller elongated loops in all phase curves reflecting two smaller periods.

CHALLENGES





Altmetric: 285

[More detail »](#)

Letter

A possible close supermassive black-hole binary in a quasar with optical periodicity

Matthew J. Graham , S. G. Djorgovski, Daniel Stern, Eilat Glikman, Andrew J. Drake, Ashish A. Mahabal, Ciro Donalek, Steve Larson & Eric Christensen

Nature **518**, 74–76 (05 February 2015)

doi:10.1038/nature14143

[Download Citation](#)

Received: 25 July 2014

Accepted: 05 December 2014

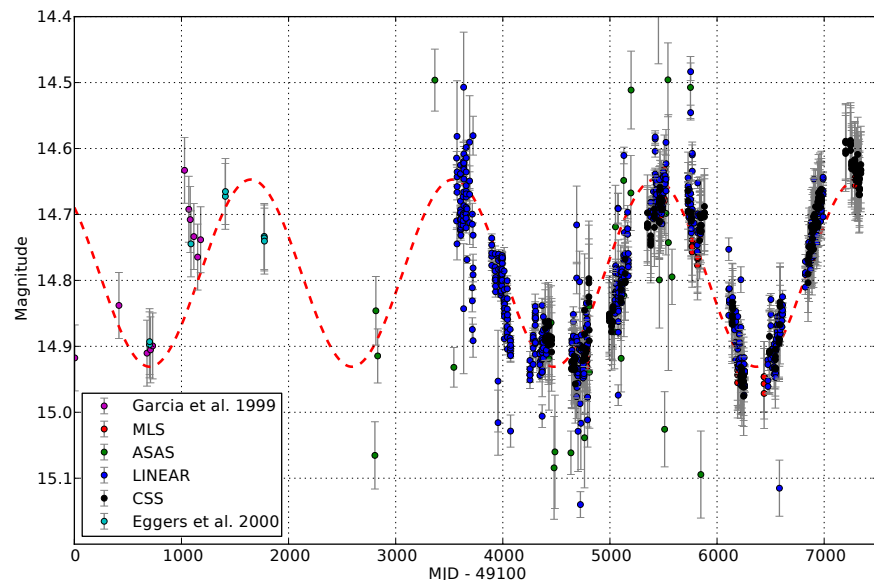
Published: 07 January 2015

Recently, Graham et al. (2015, hereafter G15) reported the detection of strong periodic variability in the optical flux of quasar PG1302-102. PG1302 is a bright (median V-band magnitude ~ 15), radio-loud quasar at redshift $z = 0.2784$, with inferred black hole (BH) mass of $10^{8.3-9.4} M_{\odot}$. The light curve in optical bands shows a quasi-sinusoidal modulation, with a best-fit period of (5.2 ± 0.2) yr and amplitude of ≈ 0.14 mag. G15 suggest that PG1302 may be a SMBHB at close separation (~ 0.01 pc), interpreting the observed periodicity as the (redshifted) orbital period of the binary.

Abstract

Quasars have long been known to be variable sources at all wavelengths. Their optical variability is stochastic and can be due to a variety of physical mechanisms; it is also well-described statistically in terms of a damped random walk model¹. The recent availability of large collections of astronomical time series of flux measurements (light curves^{2,3,4,5}) offers new data sets for a systematic exploration of quasar variability. Here we report the detection of a strong, smooth periodic signal in the optical variability of the quasar PG 1302–102 with a mean observed period of $1,884 \pm 88$ days. It was identified in a search for periodic variability in a data set of light curves for 247,000 known, spectroscopically confirmed quasars with a temporal baseline of about 9 years. Although the interpretation of this phenomenon is still uncertain, the most plausible mechanisms involve a binary system of

PG 1302-102



Graham et al. 2015

Figure 2 The composite light curve for PG 1302-102 over a period of 7,338 days (~ 20 years). The light curve combines data from two CRTS telescopes (CSS and MLS) with historical data from the LINEAR and ASAS surveys, and the literature (see Methods for details). The error bars represent one standard deviation errors on the photometry values. The dashed line indicates a sinusoid with period 1,884 days and amplitude 0.14 mag. The uncertainty in the measured period is 88 days. Note that this does not reflect the expected shape of the periodic waveform which will depend on the physical properties of the system. MJD, modified Julian day.

Did ASAS-SN Kill the Supermassive Black Hole Binary Candidate PG1302-102?

TINGTING LIU,^{1,2} SUDI GEZARI,¹ AND M. COLEMAN MILLER¹

¹*Department of Astronomy, University of Maryland, College Park, Maryland 20742, USA*

²*tingting@astro.umd.edu*

(Received xxx xx, 2018; Revised xxx xx, 2018; Accepted xxx xx, 2018)

Submitted to ApJ Letters

ABSTRACT

Graham et al. (2015a) reported a periodically varying quasar and supermassive black hole binary candidate, PG1302-102 (hereafter PG1302), which was discovered in the Catalina Real-Time Transient Survey (CRTS). Its combined Lincoln Near-Earth Asteroid Research (LINEAR) and CRTS optical light curve is well fitted to a sinusoid of an observed period of $\approx 1,884$ days and well modeled by the relativistic Doppler boosting of the secondary mini-disk (D’Orazio et al. 2015). However, the LINEAR+CRTS light curve from MJD ≈ 52700 to MJD ≈ 56400 covers only ~ 2 cycles of periodic variation, which is a short baseline that can be highly susceptible to normal, stochastic quasar variability (Vaughan et al. 2016). In this Letter, we present a re-analysis of PG1302, using the latest light curve from the All-Sky Automated Survey for Supernovae (ASAS-SN), which extends the observational baseline to the present day (MJD ≈ 58200), and adopting a maximum likelihood method which searches for a periodic component in addition to stochastic quasar variability. When the ASAS-SN data are combined with the previous LINEAR+CRTS data, the evidence for periodicity decreases. For genuine periodicity one would expect that additional data would strengthen the evidence, so the decrease in significance may be an indication that the binary model is disfavored.

observations

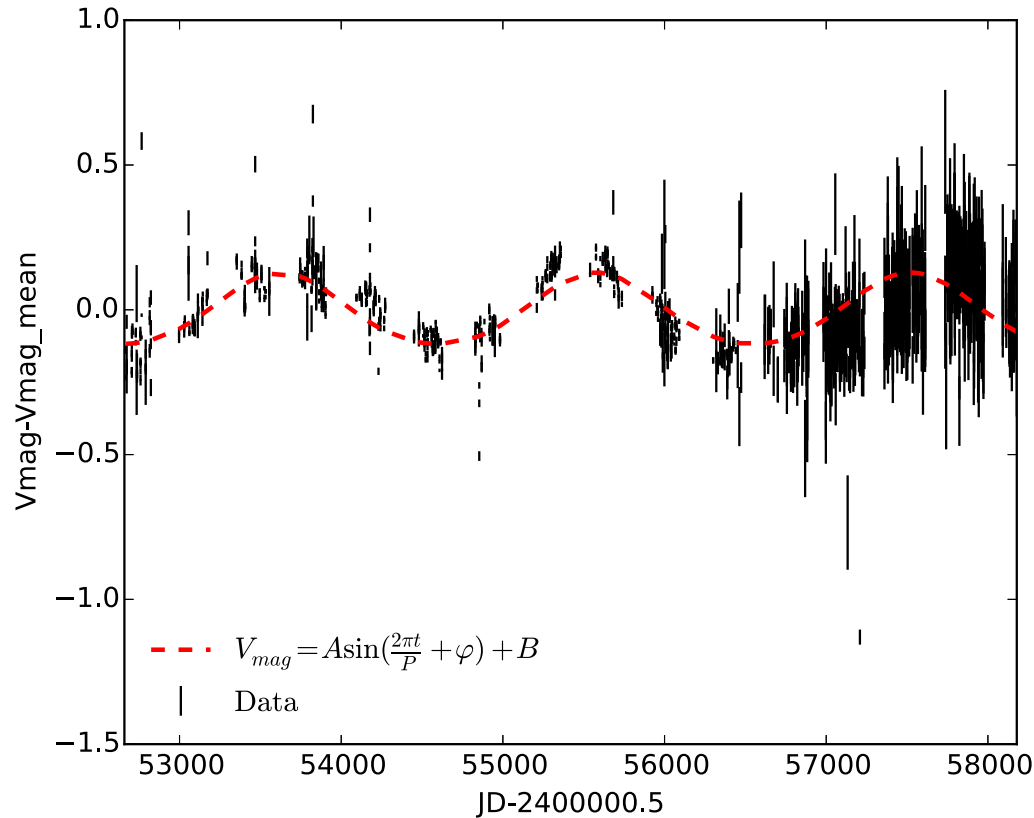
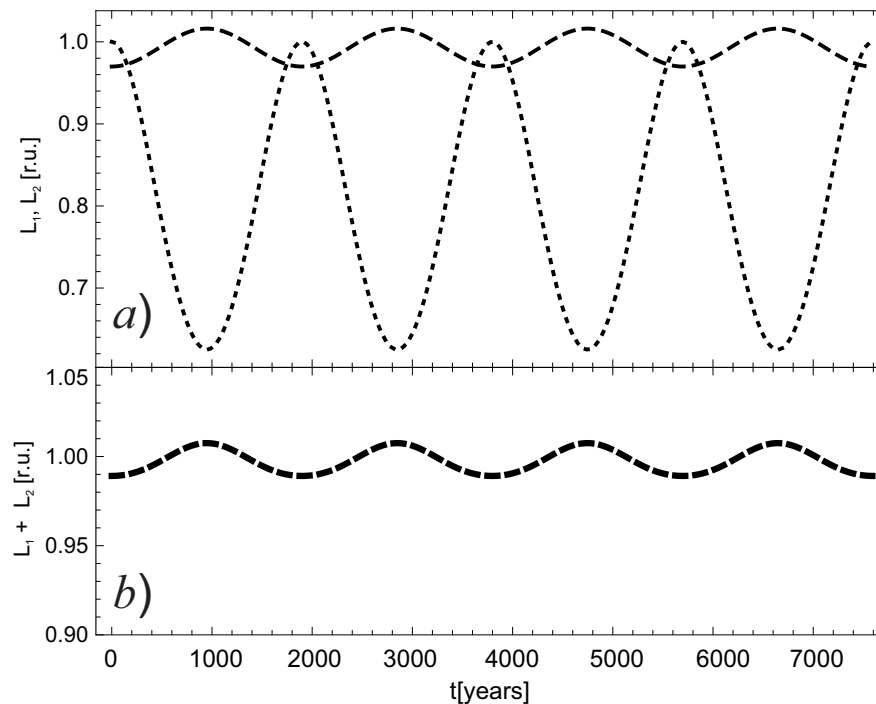


Figure 6. Best fitting of sinusoid model to the detrended (mean value is subtracted) observed light curve. Photometric magnitudes are represented by error bars whereas model with dashed, red line. The best fitting parameters are given in [Table 2](#).

unperturbed model of Binary Black Hole



Kovacevic, Popovic, Simic, Ilic 2019

Figure 1. Modeled light curve of the SMBHB system during four orbital periods (see text): (a) Individual light curves (L_1, L_2) of corresponding accretion disks of components m_1 (doted) and m_2 (dashed); (b) The modeled light curve of the total luminosity ($L_1 + L_2$) emitted from the SMBHB. The luminosity is given in relative units on y-axis, and time is given on x axis in days.

perturbed model of SuperMassive Binary Black Hole

$$T_{\text{eff}}[K] = 2 \cdot 10^5 \left(\frac{10^8}{m_i} \right)^{1/4} \left(\frac{R_{\text{in}}}{R} \right)^{\frac{3}{4}} \left(1 - \sqrt{\frac{R_{\text{in}}}{R}} \right)$$

$$T_{\text{eff}}^{\text{pert}}(R, t) = T_{\text{eff}}(R) + T_{\text{eff}}(R) \cdot \delta T(t),$$

$$\delta T(t) = P_{\text{int}} \cdot \exp \left[-\frac{(t - t_{\text{pert}})^2}{P_{\text{dur}}^2} \right]$$

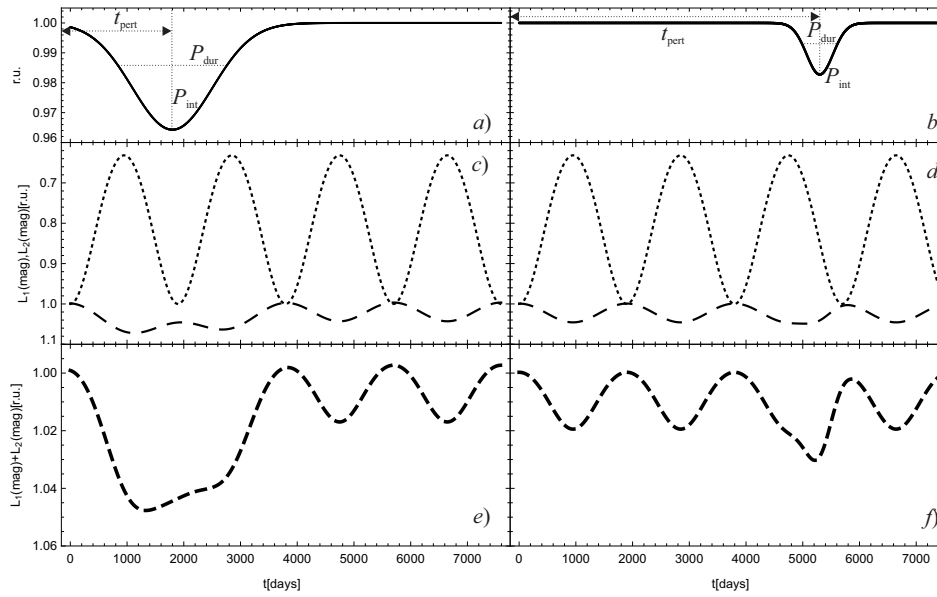


Figure 2. The influence of the different perturbations (the shapes are present in upper panels (a) and (b), see text) on the light curve of more massive component (see middle panels (c) and (d)) and the resulting light curves (shown in bottom panels (e) and (f)).

modeled perturbed curve

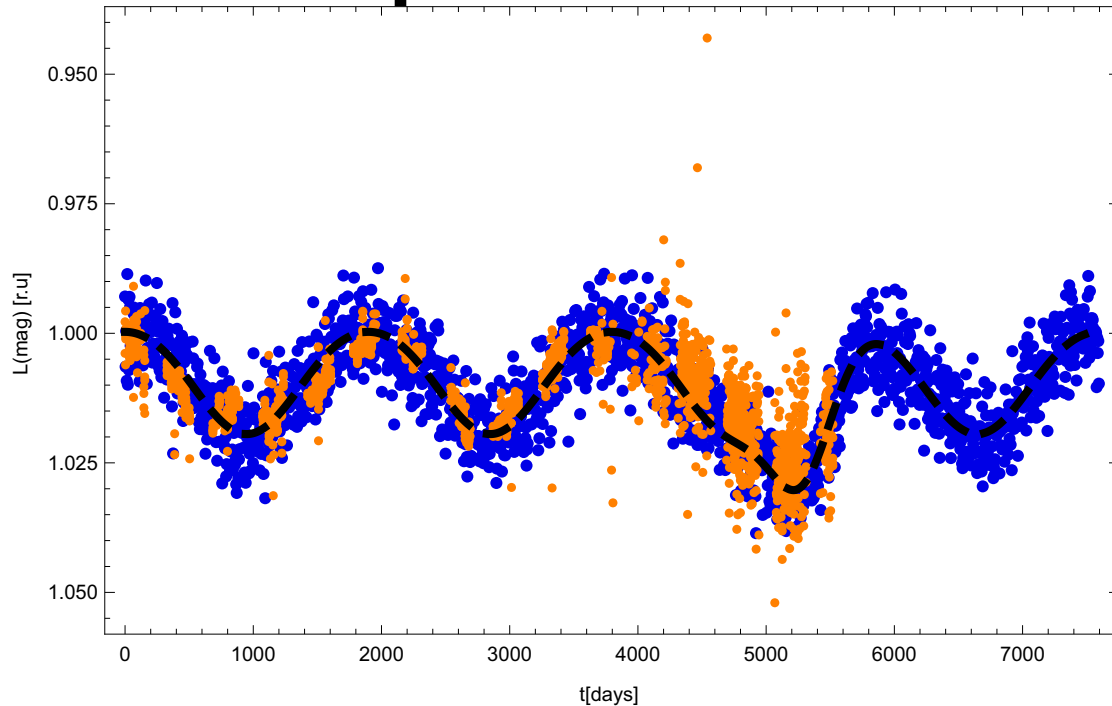


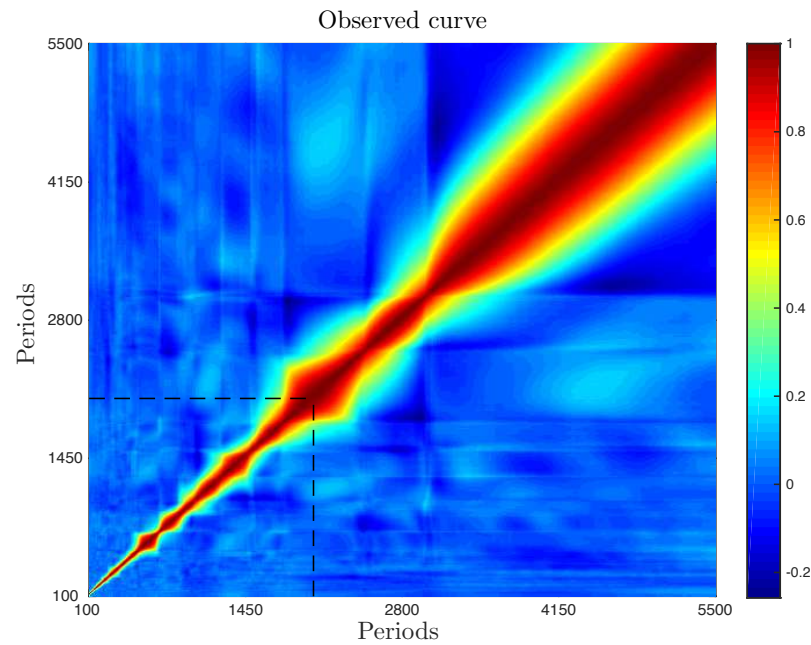
Figure 4. Observed (orange points) and modeled light curve (blue points). Dashed black line represents the modeled curve without white noise. Time is given on x-axis in days, whereas the flux (note that the observed light curve is previously expressed in magnitudes) in relative units is given on y-axis.

Table 1. Inferred parameters of the model of the SMBHB system with Gaussian perturbation in the accretion disk of the **more massive** component, defined in Section 2. Parameters AIC, BIC, AIC_{np} , BIC_{np} , and AIC_{nc} , BIC_{nc} measure the quality of perturbed, non-perturbed and pure noise model, respectively (see text).

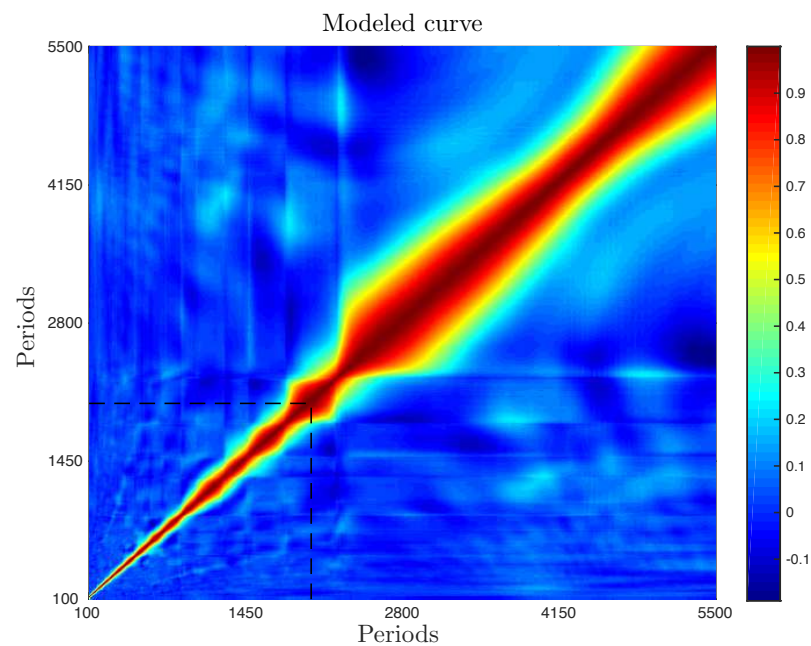
m_1 [$10^8 M_\odot$]	m_2 [$10^8 M_\odot$]	a [pc]	e	t_{pert} [days]	P_{int} [%]	P_{dur} [days]	P [days]	AIC	BIC	AIC_{np}	BIC_{np}	AIC_{nc}	BIC_{nc}
1	10	0.015	0	5300	1.7	330	1899	-4135	-4125	-3793	-3787	-3028	-3025

AN INTERPRETATION OF VARIABILITY OF PG1302-102

1972 ± 254 days



1873 ± 250 days



observations

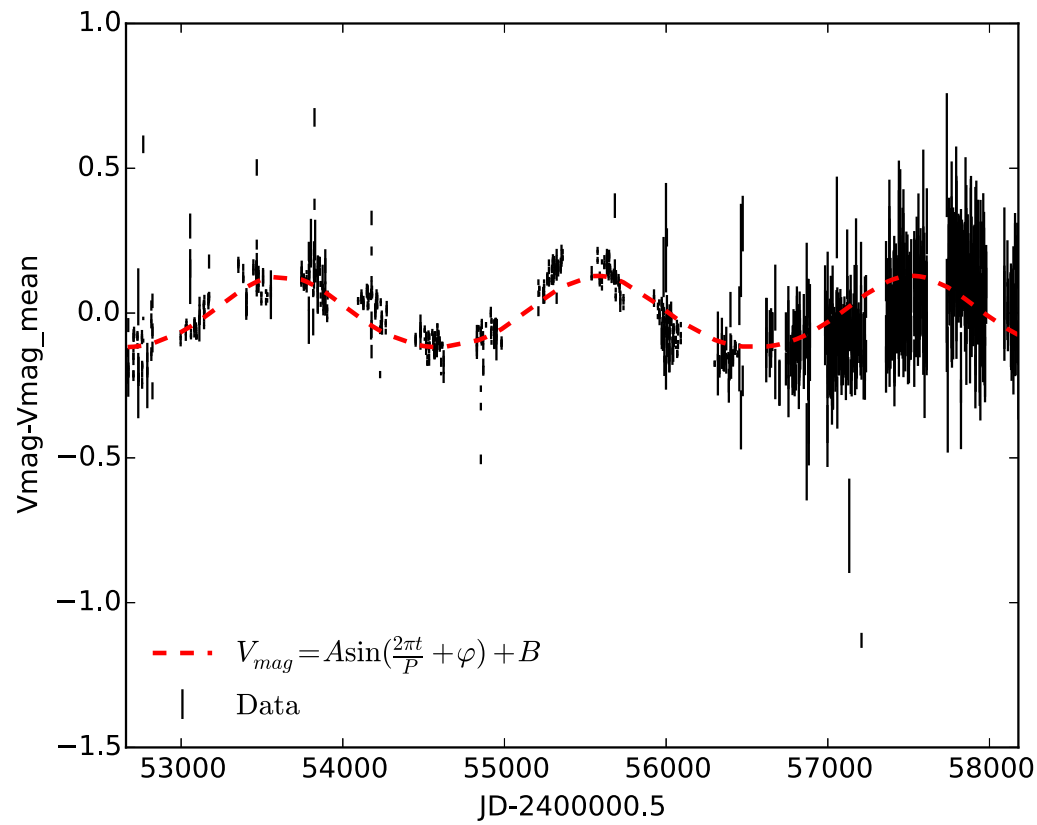
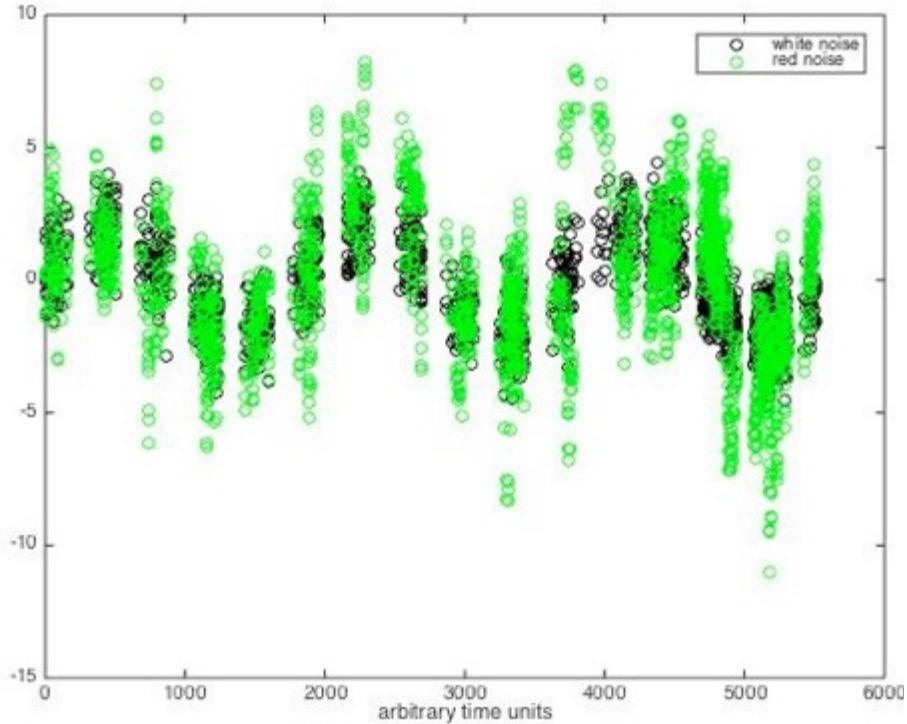


Figure 6. Best fitting of sinusoid model to the detrended (mean value is subtracted) observed light curve.

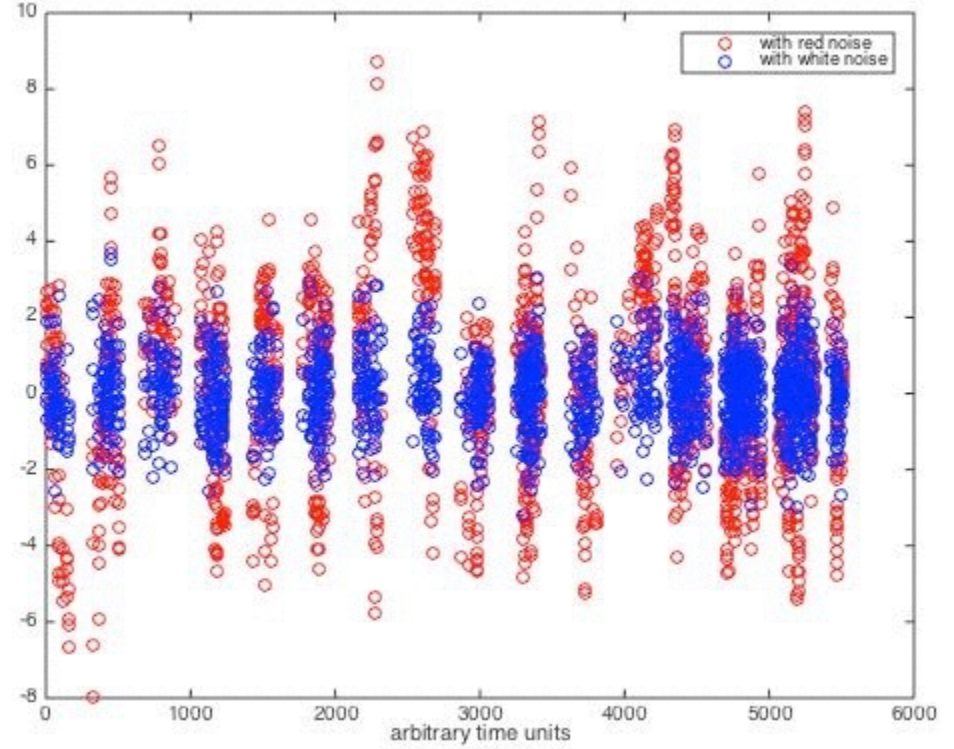
Photometric magnitudes are represented by error bars whereas model with dashed, red line. The best fitting parameters are given in Table 2.

Table 2. Best fitting parameters and their standard deviations of the sinusoid fitted to the detrended observed data, defined by Eq. 6 in Section 3. The parameters χ^2_{red} is reduced χ^2 value of the fit.

A	P [days]	φ [radian]	B	χ^2_{red}
0.123 ± 0.003	1950 ± 150	4.74 ± 0.84	-0.018 ± 0.003	1.09



red noise $+5 \cdot \sin(2\pi t / 1880)$
white noise $+ 5 \cdot \sin(2\pi t / 1880)$



red noise $+0.1 \cdot \sin(2\pi t / 1880)$
white noise $+ 0.1 \cdot \sin(2\pi t / 1880)$

SUMMARY

We develop a novel hybrid method in a search for oscillatory behavior of type I AGN. Light curves can be of arbitrary length and sampling rate, without assumption of the periodicity range. Hybrid method detects numerically periods, and produce 2D correlation maps of oscillations present in the two light curves.

Using hybrid method we show a novelty in the oscillatory patterns of the all surveys combined light curves of 5 well known type I AGN:

i) periodic variations in 3C 390.3, NGC 4151, NGC 5548 and E1821+643

ii) differences in dynamical regimes:

- binary black hole candidates:

NGC 5548 chaotic regime

E1821+643 stable regime

-double-peaked Balmer line objects:

3C 390.3 oscillatory pattern rapidly fluctuate in 2D correlation space

Arp 102B no oscillations

iii) confirmation of physical background of detected oscillations:

our coupled oscillatory models describe oscillatory behavior in the light curves